Energy & Environmental Science

Accepted Manuscript

ROYAL SOCIETY OF CHEMISTRY

www.rsc.org/ees

Cite this: DOI: 10.1039/c0xx00000x

www.rsc.org/xxxxxx

ARTICLE TYPE

Bio-inspired organic cobalt(II) phosphonates toward water oxidation

Tianhua Zhou,[abc] Danping Wang,[d] Simon Chun-Kiat Goh,[a] Jindui Hong,[ab] Jianyu Han,[a] Jianggao Mao*[c] and Rong Xu*[ab]

Received (in XXX, XXX) XthXXXXXXXXX 20XX, Accepted Xth XXXXXXXXX 20XX

DOI: 10.1039/b000000x

The development of artificial photosynthesis system that can efficiently catalyze water oxidation to generate oxygen remains one of the most important challenges in solar energy conversion to chemical energy. In photosystem II (PSII), the Mn_4CaO_5 cluster adopts a distorted coordination geometry and every two octahedra are linked by di-μ-oxo (edge-shared) or mono-μ-oxo bridges (corner-shared), which is recognized as a critical structure motif for catalytic water oxidation. These structural features provide guidance on the design and synthesis of new water oxidation catalysts. Herein we synthesized a new layered organic cobalt phosphonate crystal, $Co_3(O_3PCH_2\text{-}NC_4H_7\text{-}CO_2)_2{\cdot}5H_2O$ (**1**), and demonstrate it as a heterogeneous catalyst for water oxidation. Its catalytic activity was compared to those of cobalt phoshonates with different structures (**2**-**4**) in terms of O_2 evolution rate and O_2 yield under the same reaction condition. The compound with both mono- and di-μ-oxo bridged octahedral cobalt displays superior catalytic activity. In contrast, the presence of only mono-μ-oxo bridged cobalt in the structure results in lower O_2 yield and O_2 evolution rate. Further structural analysis reveals that the presence of longer Co-N bond induces distorted dissymmetry coordination geometry, and consequently facilitates water oxidation. These results provide important insight into the design of water oxidation catalysts.

Broader context

Splitting water into hydrogen and oxygen is a promising pathway for solar energy conversion to chemical energy. Water oxidation to oxygen (O_2) is regarded as a major challenge toward artificial photosynthesis. Recently, most water oxidation systems have been developed based on μ-oxo bridging cobalt heterogeneous water oxidation catalysts. Major advances have been made on electrochemically deposited catalytic films or colloidal suspensions of nanoparticles. Though these cobalt-based materials have been shown as promising catalyst candidates for water oxidation, it is difficult to establish the structure-performance relationship owing to their ill-defined chemical structures. In this work, we synthesized a cobalt phosphonate crystal and demonstrate its high catalytic performance for water oxidation. Comparative analysis of a series of cobalt phosphonates with different types of crystal structures reveals the potential structural features for efficient water oxidation. This study provides valuable insight into the design and synthesis of efficient water oxidation catalysts.

Introduction

Splitting water into hydrogen and oxygen is a promising and appealing solution for solar energy conversion and storage system. Water oxidation to O_2 is regarded as the bottleneck of artificial photosynthesis due to the high energy barrier for O-O bond formation. In natural photosynthesis, photosystem II (PSII) is responsible for biocatalytic water oxidation.[1] More recently, single-crystal X-ray crystallography at a resolution of 1.9 Å reveals that the heart of PSII is the oxygen evolving complex (OEC) containing the active Mn_4CaO_5.[2] In this cluster, every two metal atoms are linked by di-μ-oxo (edge-shared) or mono-μ-oxo bridges (corner-shared), which are recognized as a critical structural component responsible for catalytic water oxidation.

The development of bio-inspired catalysts to efficiently capture solar energy is one of the main challenges to attain a renewable and sustainable energy system.[3-6] To closely mimic the chemical function of PSII, many multinuclear μ-oxo manganese complexes are studied as models of the OEC, among which only a few have shown activity toward water oxidation.[7, 8] Although precious metal oxides such as IrO_2 and RuO_2 have been regarded as the most effective water oxidation catalysts (WOCs), the development of efficient artificial PSIIs based on low cost earth-abundant elements is more appealing. Recently cobalt-based catalysts have been shown to be promising catalyst candidates for water oxidation.[9-13] Among them, great efforts have been devoted to catalysts possessing Co_4O_4 cubanes, analogous to the active sites of PSII, such as organic cobalt complexes,[14-17] inorganic polyoxometalate (POM) cobalt complexes,[18-20] Co_3O_4,[21] and $Li_2Co_2O_4$.[22] The cubic Co_4O_4 core is regarded as the crucial structural feature for efficient catalysis of water oxidation. Interestingly, some cobalt solid catalysts without Co_4O_4 topology have also been reported toward catalyzing water oxidation. For example, the Co-based perovskite catalyst displays an electrocatalytic activity in water oxidation reaction in alkaline solution.[23, 24] Recently, Co-Fe Prussian blue-type coordination polymer was developed as bimetallic electrocatalysts for water

oxidation in neutral media.[25]

Additionally, various amorphous cobalt phosphate materials have also been investigated as WOCs. For example, Nocera and co-workers developed the *in situ* electrodeposited Co-Pi film (CoO_x/PO_4) from Co(II) ions in phosphate buffer solution (pH 7.0) that can act as an efficient electrocatalyst for water oxidation with a low overpotential of 410 mV.[26] Although the Co-Pi catalyst film lacks the long-rang crystal order, using X-ray adsorption spectroscopy (XAS), Dau's group found that the central structural unit is composed of clusters of interconnected complete or incomplete Co_4O_4 cubanes.[27] Nocera and co-workers showed that layered Co-Pi possesses the Co oxo/hydroxo clusters comprised of edge-sharing CoO_6 octahedra based on the extended X-ray absorption fine structure (EXAFS) spectra. Computational studies showed that the layered Co-Pi materials contain both corner- and face-sharing cubane units in the same crystallite.[28] Similarly, the group of Thapper and Styring also found that cobalt phosphonates formed *in situ* from a mixture of cobalt and methylenediphosphonate (Co/M2P) can catalyze water oxidation in an aqueous solution at pH 7.0 under visible light irradiation.[29] However, the structure of such a colloidal catalyst still remains uncertain.[30] In addition, Tilley and co-workers developed a thermolytic molecular precursor method to prepare cobalt metaphosphate nanoparticles $Co(PO_3)_2$ which exhibited a much lower onset overpotential than those of Co-Pi film and Co_3O_4.[11] They proposed that the high catalytic activity could be attributed to cobalt oxide species on the surface. Thus, it is highly desirable to develop suitable alternatives to cobalt phosphate or phosphonate materials that display efficient catalytic activity and possess well-defined crystal structure. The well-defined crystal structure may allow us to obtain precise knowledge about the distribution and local geometrical environment of catalytic sites.[31]

Herein, we synthesized a new cobalt phosphonate hybrid $Co_3(O_3PCH_2\text{-}NC_4H_7\text{-}CO_2)_2{\cdot}4H_2O$ (**1**) and determined its crystal structure by single-crystal X-ray diffraction analysis. It is composed of μ-oxo bridging cobalt clusters edge-sharing CoO_6 octahedra without Co_4O_4 topology, closely imitating the structure and function of the natural PSII complex, and identified as efficient molecular heterogeneous catalysts for photocatalytic water oxidation under visible light irradiation. To the best of our knowledge, there has been no attempt to study the photocatalytic water oxidation based on cobalt cluster-based phosphonate hybrid materials. We found that the presence of longer Co-N bond induces distorted dissymmetry coordination geometry, and consequently facilitates water oxidation.

Experimental Section

Visible light driven water oxidation

Photocatalytic oxygen evolution was carried out in a top window Pyrex reactor connected to a closed gas circulation and evacuation system. In a typical run, the aqueous reaction solution (10 mL) containing cobalt phosphonates (**1-4**) (1.4 mg), [Ru(2,2'-bipyridine)$_3$]Cl_2 (1.0 mM), $Na_2S_2O_8$ (5.0 mM) and sodium borate buffer (40 mM) at pH 9.0 was irradiated using a 300 W Xe lamp (Newport) equipped with a 420 nm cutoff filter. The light intensity at the surface of the reaction solution was measured to be 210 mW/cm^2. The temperature of the reactor was kept at about 20 °C by a cooling water jacket. The O_2 generated in the headspace was measured by an online gas chromatography (Shimadzu GC-2014, TCD detector, argon as carrier gas, molecular sieve 5Å column). A baseline was recorded for each experiment to confirm the absence of air in the system. Before the reaction and materials characterization, the as-synthesized crystal samples were grinded using the pestle until a homogenous fine powder was obtained, which is crucial to ensure experimental reproducibility. To evaluate the effect of the surface area, the photocatalytic activities of the as-synthesized crystal samples without grinding were also obtained. All the rest of the experiments and characterization were carried out using the powder samples unless otherwise specified. After the photocatalytic reaction, the samples (**1-4**) were recovered by centrifugation at 20,000 rpm and washed several times with deionized water, ethanol and acetone till the solution was colorless. The recovered samples were further characterized and reused for the second run of the photoreaction. Different band-pass filters (centered at 420, 440, 460, 480, and 500 nm) were equipped to conduct reactions under photons of different wavelengths and collecting quantum efficiency (QE) results. The QE of O_2 formation is defined as the number of O_2 molecles formed per two absorbed photons.[32] The amount of O_2 evolved in the initial 10 min was used to calculate QE using the equation below. The number of photons from irradiation was measured using a photodiode.

$$\mathrm{QE} = \frac{2 \times \text{the number of evolved oxygen molecules}}{\text{the number of incident photons}} \times 100\%$$

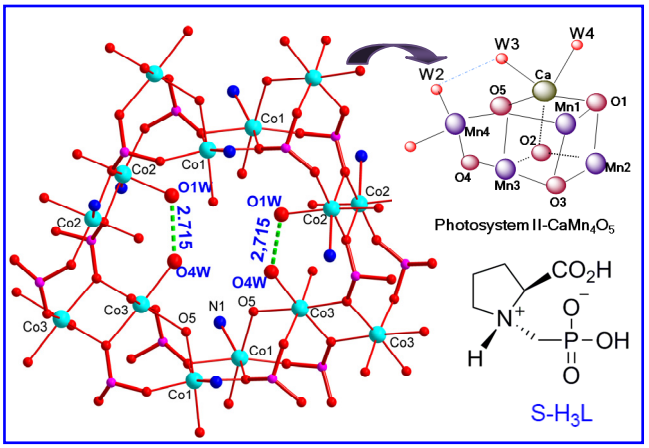

Fig. 1 Ball and stick view highlighting the connectivity of the pairs of cobalt octahedra for **1**. Co, O, P, and N are shown as cyan, red, magenta, blue, respectively (where, S-H_3L = $H_2O_3PCH_2\text{-}NC_4H_7\text{-}CO_2H$).

Isotope-labelled experiment

The $^{18}OH_2$ labelling experiments were performed using ^{18}O enriched water (16.8 vol%) under the similar photocatalytic reaction conditions. $^{18}OH_2$ (1.73 mL) was added to a flask followed by adding an appropriate amount of $Na_2S_2O_5$ (12.7 mg), [Ru(2,2'-bipyridine)$_3$]Cl_2 (7.4 mg), catalyst **1** (5.2 mg), and borate buffer solution (5 mL, 80 mM, pH 9.0). The flask was sealed after the addition of deionized H_2O to reach a total volume of 10 mL reaction solution with stirring. The flask was then evacuated to ensure air removal and followed by purging with

helium to the normal pressure. After irradiation of 60 min, 100 μL of the O_2 gas generated in the headspace was withdrawn using a SGE gas-tight syringe and then injected into a GC-MS (Agilent, GC Model 6890/MS Model 5973) with a molecular sieve 5Å column and an electron impact ionization mode to focus on the m/z in 30-50 range. The single ion mode was used to scan for the ions with m/z of 28, 32, 34 and 36. The relative concentrations of ions were determined by integrating the area under the signal of the appropriate extracted m/z values.

Results and Discussion

Layered cobalt phosphonates were prepared by hydrothermal methods (ESI†). Single-crystal X-ray diffraction analysis revealed that **1** crystallizes in monoclinic space group *C2/c* and features a two-dismensional layered architecture. The asymmetric unit of **1** contains three unique Co(II) ions, two S-L^{3-} anions and four aqua ligands (Fig. S1a†). Both Co1 (CoO5N) and Co2 (CoO5N) are octahedrally coordinated by three phosphonates oxygen atoms, one carboxylate oxygen atom from three S-L^{3-} anions, one nitrogen atom from one S-L^{3-} anion as well as one aqua ligand. Co3 (CoO6) is octahedrally-coordinated by three phosphonate oxygen atoms and one carboxylate oxygen atom from four S-L^{3-} anions as well as two aqua ligands (Fig. S1a†). The two S-L^{3-} anions in 1 are heptadentate and bridged with five Co ions. They adopt two different types of coordination modes (Fig. S1b). In the S-L^{3-} anion containing P1 atom, two phosphonate atoms are unidentate, whereas the remaining two phosphonate and carboxylate atom each is bidentate. In the S-L^{3-} anion containing P2 atom, two phosphonate oxygen atoms are bidendate whereas the remaining phosphonate and carboxylate atom each is unidentate. Pairs of di-μ-oxo bridged edge-sharing CoO_6 and CoO5N cobalt octahedra are linked *via* corner-sharing oxygen atom (O5) into Co-O chains consisting of cubane-like Co_4O_5 unit along the *c*-axis (Fig. 1 and Fig. S1c†). These chains are further connected into two dimensional (2D) layered structure by organic ligands and di-μ-oxo bridged Co2 atom dimers (Fig. S1d†). The organic groups of the S-H_3L ligands are orientated toward the interlayer space. These 2D layers are held together *via* weak van der Waals force (Fig. S1e†). All the selected bond lengths are provided in Tables S1-3 (ESI†). In the cluster, the nearest distance of Co···Co by di-μ-oxo bridge is 3.196 (1) Å and the longest is 3.270 Å. The Co-Co distance averaged over all edge-sharing octahedral cobalt atoms is 3.244Å. The Co-O distances are in the range from 2.006 (3) to 2.199 (3) Å, whereas the Co-N distances are in the range from 2.209 (3) to 2.256 (4) Å. All the cobalt atoms in the structure display distorted octahedral coordination geometry and are in the divalent state as confirmed by the X-ray photoelectron spectrum (XPS) (Fig. 3). To further explore the interplay between the molecular structure and catalytic activity, cobalt phosphonates with different structures including $Co_3(O_3PCH_2\text{-}NC_4H_7\text{-}CO_2)_2{\cdot}4H_2O$ (**2**), $Co_3(O_2C\text{-}CH_2CH_2\text{-}PO_3)_2{\cdot}6H_2O$ (**3**), and $Co(PhPO_3)(H_2O)$ (**4**) were synthesized by hydrothermal methods according to the reported methods (ESI†). The structure and the phase purity of all the cobalt phosphonates (**1-4**) were verified by X-ray diffraction (XRD) (Fig. 3 and Fig. S2-8) and elemental analysis (EA) (ESI†). In addition, it is well known that Co_3O_4 is an excellent WOC under visible light irradiation.[21, 29, 33-35] Thus, 20 nm-sized Co_3O_4 was also synthesized as a reference material according to the method reported.[36] The phase purify was verified by XRD and morphological properties by TEM analysis (Fig. S9†).

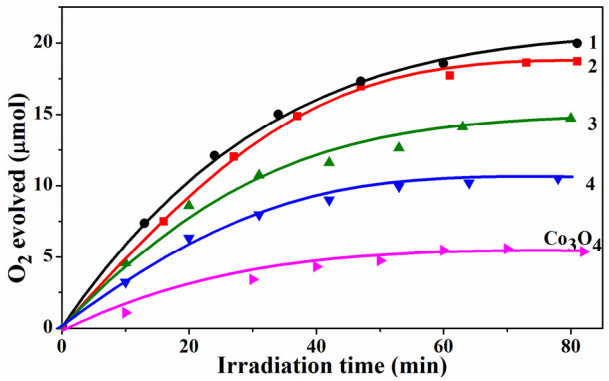

Fig. 2 O_2 evolution over different cobalt phosphonates (**1-4**) and Co_3O_4 control (0.14 g L^{-1}). Conditions: 1.0 mM $[Ru(bpy)_3]^{2+}$, 5.0 mM $Na_2S_2O_8$, 40 mM borate buffer (initial pH 9.0), total volume of the reaction solution 10 mL, light source: 300 W Xe lamp with 420 nm cut-off filter.

Considering that Ru(II)(2,2'-bipyridine)$_3^{2+}$ as a photosensitizer is subject to the photoinitiated decomposition due to the population of the low-lying *dd* states, to minimize the photodecomposition of the Ru(II)(2,2'-bipyridine)$_3^{2+}$, the utilization of buffer solution is required.[37] Thus, the catalytic activity of the cobalt phosphonates for photon-driven water oxidation was investigated according to the standard method reported by using $[Ru(bpy)_3]Cl_2$ as the photosensitizer, $Na_2S_2O_8$ as the sacrificial oxidant, and sodium borate solution (pH 9.0) as the buffer solution under visible light ($\lambda > 420$ nm).[38-40] Oxygen evolution was monitored by an on-line gas chromatography. During water oxidation, the sacrificial oxidant $Na_2S_2O_8$ acts as a two-electron acceptor. This suggests that the theoretical amount of O_2 produced should correspond to half the amount of persulfate used.

Table 1. Photocatalytic water oxidation activities of cobalt phosphonate catalysts synthesized in this work.

Catalyst	R_{O2} (μmol s^{-1} g^{-1})[a]	O_2 yield (%)[b]	Avg. Co-Co distance, Å (edge-sharing octahedra)	Avg. Co-X(X = O, N) distance, Å (cobalt coordination geometry)
1	7.1±0.2	78±2	3.244	2.122
2	5.8±0.2	77±2	3.245	2.113
3	5.1±0. 3	57±4	3.165	2.102
4	3.9±0. 3	44±3	N.A	2.129

[a]O_2 evolution rate (normalized by the catalyst mass) after irradiation for 10 min; [b]O_2 yield = (mole of O_2)/(1/2×mol of $Na_2S_2O_8$).

All the remaining oxygen evolution experiments were performed under the same optimized reaction conditions including pH 9.0 and the concentrations of the buffer (40 mM), $[Ru(bpy)_3]Cl_2$ (1.0 mM) and $Na_2S_2O_8$(5.0mM). After the reaction, the pH values were determined and listed in Table S5. In addition, control experiments showed that no O_2 evolution can be observed from reaction solutions in the absence of either one of the four critical components, cobalt phosphonates, photons,

$[Ru(bpy)_3]Cl_2$ and $Na_2S_2O_8$. To confirm the formation of molecular oxygen from water by photocatalysis, an isotope-labelling water oxidation experiment was performed with **1** as the catalyst. The water was enriched with 16.8% of $^{18}OH_2$. The experimental oxygen distribution of $^{16}O^{16}O$: $^{16}O^{18}O$: $^{18}O^{18}O$ was determined to be 70.1: 26.9: 3.0 (Fig. S10†), which is consistent with the theoretical distribution of 69.2: 28.0: 2.8. This observation indicates that oxygen evolved is catalytic in nature.

Figure 2 shows that O_2 evolution with cobalt phosphonate materials increases steadily with irradiation time, and then gradually reaches the maximum at around 60 min. The turn-over number (TON), initial turnover frequency (TOF), O_2 evolution rate (R_{O2}) and O_2 yield obtained for all the samples are summarized in the Table 1 and Table S4†. For **1**, the amount of O_2 evolved after 80 min is 20 μmol, which is larger than that of Co_3O_4 (5.39 μmol). The initial R_{O2} for **1** after irradiation of 10 min is 7.1 μmol s^{-1} g^{-1} which is significantly higher than that of Co_3O_4 (2.1 μmol s^{-1} g^{-1}). The R_{O2} is also better than that of the similarly sized Co_3O_4 (4.8 μmol s^{-1} g^{-1}) reported in the literature.[33]

To further quantify the photocatalytic performance, on the orther hand, the O_2 chemical yields (Q_{CY}) were also calculated. The O_2 yield (78±2%) obtained from **1** is higher than that from Co_3O_4 (21±3% from this work at pH 9.0) and comparable to those reported for catalysts containing precious metals such as IrO_2 particles (69%, pH 5.0)[41], and cobalt-based heterogeneous catalysts such as $LaCoO_3$ particles (74%, pH 7.0),[24] colloidal cobalt phosphonate (about 50%, pH 7.0),[29] and Co_3O_4 (64% at pH 8.0).[33] In addition, the O_2 yield of **1** is also comparable to those of highly active homogeneous cobalt-based catalysts at the same pH of 9.0.[39, 40] Furthermore, the QE of O_2 evolution under light irradiation of different wavelength was measured. Before collecting the QE data, the steady-state luminescence quenching of $[Ru(bpy)_3]^{2+*}$ formed by photoinduction was investigated under the conditions similar to those in Fig. 2. In the absence of the catalyst, it was found that 51% of the excited state can be quenched by persulfate by comparing the emission intensity values in the presence and absence of persulfate (Fig. S11).[42] Upon addition of the catalyst, the quenching efficiency is not affected significantly by both **1** and Co_3O_4, indicating that the charge transfer between the photosensitizer and the catalyst may not be the rating limiting factor. The similar phenomenon was reported for a system containing a polyoxometalate catalyst using $[Ru(bpy)_3]^{2+}$ photosensitizer and persulfate electron acceptor.[32] Under such a circumstance, the QEs of O_2 evolution could reflect the activity of the catalyst as one of the major limiting factors. The QE data measured are shown in Fig. S12. The highest QEs of **1** and Co_3O_4 were measured to be about 25 % and 12% at 460 nm, respectively. The QE of **1** is as high as those of other cobalt-based catalysts reported.[19, 43]

Nevertheless, it is difficult to obtain a definite conclusion by directly comparing the chemical yield and QE, which can be influenced by diffusion of the photosensitizer and oxidant, and the concentration of catalyst, persulfate and photosensitizer, among different water oxidation systems in other work under different reaction conditions.[35, 44, 45] In particular, the measured data depend on the sensitizer-catalyst particle interaction at different pH values to a substantial extent.[46] Nevertheless, the results here corroborate that **1** is an efficient catalyst. Considering the heterogeneous catalytic process, an apparent TOF normalized to the surface area was further evaluated. The R_{O2} calculated from the initial slopes (10 min) of the kinetic curves were then normalized using the Brunauer-Emmett-Teller (BET) surface areas obtained by N_2 adsorption measurements at 77 K. It was found that the apparent TOF of **1** was calculated to be 0.30 $\mu mols^{-1}$ m^{-2} which is significantly higher than those of Co_3O_4 at 0.03 μmol s^{-1} m^{-2} from this work. Furthermore, the photocatalytic activities of the as-synthesized crystal samples (**1-4**) were investigated under the same reaction conditions. Compared to the respective powder samples, the crystal samples with lower surface areas display lower yield and R_{O2} (Fig. S16 and Table S6†). Although the activity data do not show a linear dependence to the surface area due to the complexity introduced by other factors such as sensitizer/oxidant−particle interaction, these observations indicate that higher catalytic activity can be resulted if more active sites can be accessed by reducing the particle size and exposing a larger surface. As a consequence, the relationship between the structure and performance for cobalt phosphonates would require extensive structural analysis.

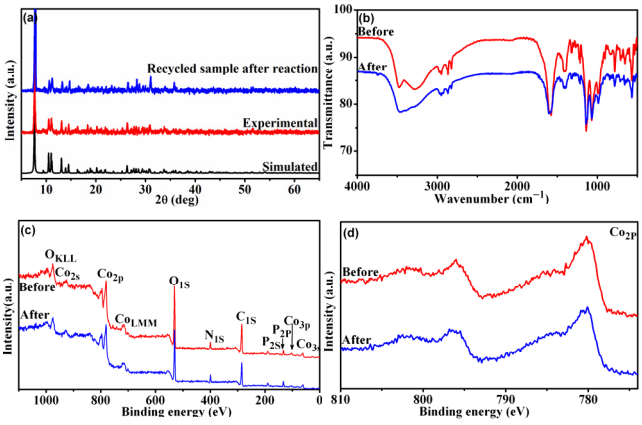

Fig. 3 XRD (a), IR (b), XPS survey (c) and Co 2p region of the XPS spectrum (d) of **1** before and after photoreaction.

To explore potential structural features of cobalt phosphonates required for effective water oxidation, three additional layered cobalt phosphonates **2-4** were also examined. Fig. 2 shows the kinetics of O_2 evolution with **2**, **3** and **4** under visible light irradiation (Table S4†). The amount of O_2 evolved from **2** (18.7 μmol) containing the similar corner-sharing (mono-μ-oxo bridging) and edge-sharing (di-μ-oxo bridging) octahedral cobalt to **1** is close to that of **1** (20 μmol). While the amount of O_2 evolved from the reaction solution with **3** (14.7 μmol) consisting of only edge-sharing (di-μ-oxo bridging) octahedral trinuclear cobalt is smaller than those from **1** and **2**. However, when mono-μ-oxo bridging mononuclear cobalt phosphonate was employed as catalyst, the amount of oxygen evolved (10.7 μmol) from **4** was found to be 50% lower than that of **1**. Accordingly, the O_2 evolution rate and O_2 yield obtained from **1-4** are in the order of **4** < **3** < **2** ≈ **1**. Furthermore, the trend is not altered when as-synthesized crystal samples were used as the catalysts (Fig. S16 and Table S6†).

Considering the highly oxidative conditions during

photoreaction, there exists possibility of ligand oxidation leading to catalyst degradation. Molecular catalysts have been often reported to decompose to metal oxides as the real catalysts. In order to probe the stability of cobalt phosphonates, samples recycled after photocatalytic reaction were further characterized. A combination of XRD and IR measurements confirm the maintenance of the cobalt phosphonates framework (Fig. 3a-b). However, an important concern is that a small amount of highly active metal oxides including cobalt oxides or RuO_2 could be responsible for the observed high activity of **1**. Considering that XPS measurement is surface-sensitive, the surface composition before and after photocatalytic reaction was observed by XPS (Fig. 3c-d, Fig. S17†). In agreement with the results of IR and XRD, after 2 h of reaction the spectrum of **1** remains unchanged compared with that of the as-prepared sample (Fig. 3c). Fig. 3d displays the binding energy of $2p_{1/2}$ and $2p_{2/3}$ XPS peaks for Co at 780.2 and 796.0 eV, respectively, with satellite peaks at 784.1 and 802.1 eV before reaction. The same binding energies of Co 2p were found for the recycled sample indicating that there is no change in the valence state of Co(II). Furthermore, no peak was observed in the Ru 3d region, confirming no detectable RuO_2 formed on the catalyst. Though the above characterization results have confirmed the stability of the bulk structure, whether the activity of **1** could derive from an amorphous cobalt oxide phase[47] or newly formed surface phase during photocatalysis remains a concern.[48] To verify the speculation, all recycled cobalt phosphonates were further subjected to HRTEM analysis (Fig. S18†). Representative HRTEM images of the surface regions of **1** before and after photocatalytic reaction are shown in Fig. 4. The lattice fringes in the images of samples both before and after photoreaction are visible up to the surface boundary without any amorphous layers. Furthermore, the FFTs of the catalysts (Fig. S18†) are basically consistent with its crystal structure. Such observations indicate no evidence of any phase transformation during the photocatalysis, supporting that the surface active sites are derived from the underlying crystal structures.

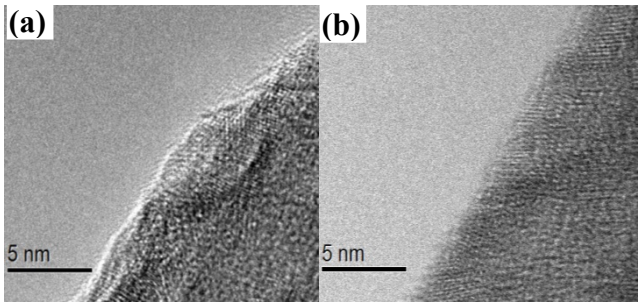

Fig. 4 HRTEM images of surface regions of **1** before (a) and after photocatalysis (b).

Recently, the stability of molecular WOCs has received extensive attention. One of the main concerns is that WOCs could dissocitate into soluble homogeneous species.[49] To evaluate the amount of dissolved cobalt species, the reaction solution was measured by inductively coupled plasma mass spectrometry (ICP-MS) after removal of the solid particles at the end of the photocatalytic reaction. The analysis results indicated that less than 2.4% of cobalt in the catalysts dissolved into the reaction solution. Detailed results and the procedure are provided in the Supporting information (Table S7†). To further verify whether this small amount of dissolved cobalt species is responsible for the observed catalytic activity, control experiments were performed. Considering that no suitable soluble cobalt phosphonates complexes are available, a commonly used candicate for the in situ generated species is free Co(II) ions for cobalt-based WOCs system, althought it is probably different from the complex form.[14, 17, 18, 20, 39, 40, 50] In this work, $Co(NO_3)_2$ was also employed as a reference species. By adding of 5 mol% or 10 mol% of $Co(NO_3)_2$ to the reaction system of **1**, it was found that the added Co(II) species has no effect on the kinetics or yield of oxygen evolution (Fig. S19†), thus supporting that the homogeneous cobalt species cannot account for the observed activity of **1**. On the other hand, we reused the recycled samples under the same initial reaction conditions. The O_2 yield of **1** did not drop significantly in the recycle run (Fig. S20†). These observations indicate that **1** acts as a stable molecular heterogeneous catalyst responsible for high water oxidation activity. The stability of all the other three cobalt phosphonates was also confirmed by XRD, IR, XPS, HRTEM and recycle study (Figs. S5-8†, Fig. S13†, Fig. S17†, Fig. S18†, and Fig. S20†).

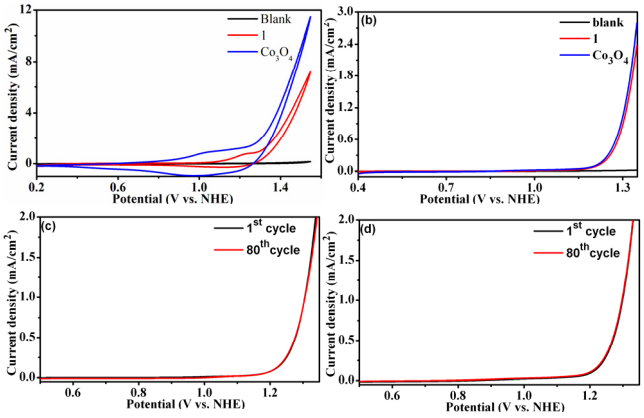

Fig. 5 (a) CV curves with Co_3O_4 (blue), **1** (red) and without catalyst (black) (scan rate, 20 mV/s), (b) LSV curves of **1** and Co_3O_4 (scan rate, 2 mV/s), LSV curves of (c) **1** and (d) Co_3O_4comparing the initial and the 80th scans (scan rate, 2 mV/s). All results were obtained in 0.1 M phosphate buffer solution (pH 7.0).

Considering that the electrochemical properties of most cobalt-based materials were studied in phosphate buffer solution at pH 7.0, here the electrochemical experiments including cyclic voltammetry (CV) and linear sweep voltammogram (LSV) were firstly performed with the glassy carbon working electrode coated with **1** in 0.1 M phosphate buffer solutions at pH of 7.0. To prevent the drop of pH and maintain an ionic strength of buffer solution,[51] specially to avoid the accumulation of oxygen bubbles resulting in the drop of catalysts from the electrode, all measurements were carried out on a rotating disk electrode (RDE) at a rotating rate of 1600 rpm. For comparison, the electrocatalytic properties of Co_3O_4 were also examined. As shown in Fig. 5a, the CV of **1** shows an Co(III)-OH/Co(II)-OH_2 oxidation wave at E_p of 1.22 V (E_p is the peak potential) versus the normal hydrogen electrode (NHE). The oxidation wave is followed by the onset catalytic wave at 1.30 V. It was shown that

the overpotential (η) of **1** occurs at around 484 mV, generating an anodic current density of 1 mA/cm^2 (Fig. 5b), which is higher than the overpotential of the precious metal-based nanoparticles IrO_x (η = 250 mV average) at the same current density.[52] However, the value is comparable to that of the extensively investigated Co_3O_4. As shown in Fig. 5b, the Co_3O_4 electrode shows a similar LSV to **1**, which generates an anodic current density of 1.0 mA/cm^2 at 1.29 V vs NHE, corresponding to an overpotential of 481 mV. However, there is significant difference between the CV curves of **1** and Co_3O_4 having large chemical capacitance (Fig. 5a), ruling out the presence of the same surface phase in the two samples.[17] The stability of **1** and Co_3O_4 was confirmed by LSV, scanning from 0.4 to 1.54 V versus NHE for 80 cycles (Fig. 5c-d), which shows that **1** afforded almost a similar LSV curve after 80 cycles. Furthermore, constant potential electrolysis experiments were carried out at an applied potential of 1.3 V versus NHE. The current densitie versus time are shown in Fig. S22. It can been seen that for all phosphonate samples the current densities remian relatively constant after a slight initial decrease which is probably due to partial blocking of the active sites of the catalysts by the O_2 bubbles formed.[53] These observations indicate that the electrocatalytic activity and stability are comparable to those of Co_3O_4. Moreover, the catalytic performance of **1** also compares favorably with other excellent water oxidation catalysts reported in neutral media. For example, Co-Pi catalyst was reported to generate 1 mA/cm^2 at 1.23 V versus NHE (η = 410 mV) on ITO in 0.1 M phosphate buffer solution at pH 7.0. We also noted that a lower onset overpotential was determined to be 313 mV for cobalt metaphosphate $Co(PO_3)_2$, but with the corresponding current density below 1 mA/cm^2. More recently, electrocatalytic properties of spinel-type $ZnCo_2O_4$ and Co_3O_4 were reported.[54] Both $ZnCo_2O_4$ and Co_3O_4 catalysts were reported to generate 1 mA/cm^2 at 1.71 V versus RHE (η = 480 mV) in 0.1 M phosphate buffer solution (pH 7.0). Their Tafel slopes from LSV were determined to be 85 and 76 mV/decade, respectively.[54] Similar Tafel slopes for **1** (83 mV/decade) and Co_3O_4 (81 mV/decade) were also obtained from our LSV. In an attempt to obtain more accurate Tafel slopes, the steady state data were also collected (Fig. S21†, Table S8†). However, the Tafel slopes obtained from the steady state data are as high as those collected from LSV. Such results suggest that the reaction may be subjected to mass transport limitation.[51] Well-buffered electrolytes could be required.[51]

The electrochemical behaviour of **1** in 0.04 M (40 mM) borate buffer solution was also studied (Fig. S23†). The current of CV slightly increased after 40 cycles. However, we noted that the CVs remained unchanged at a scan rate of 100 mV/s during continuous potential cycling from 0.2 to 1.4 V versus NHE, indicating that **1** is stable in borate buffer solution. The overpotential at 1 mA/cm^2 and Tafel slopes from steady state data have also been determined (Table S8†). As expected, the slope (68 mV/decade) is close to that of Co-Pi film (60 mV/decade),[55] thus demonstrating the improved electrocatalytic activity in borate buffer solution (pH 9.0) compared to that in phosphate buffer solution (pH 7.0). The water oxidation properties of **2-4** were also examined (Fig. S21†). All the samples show the similar Tafel slopes and their overpotential followed the same trend observed for photocatalytic water oxidation. Co_3O_4 displays a similar overpotential and Tafel slope to **1** but lower photocatalytic activity for oxygen evolution, which was probably resulted from the aggregation of the active sites in solution system.[56] By contrast, the metal-organic framework of organic cobalt phosphonates chemically separates the catalytic centers from aggregation, similar to the funciton of a support material such as Al_2O_3 reported.[56]

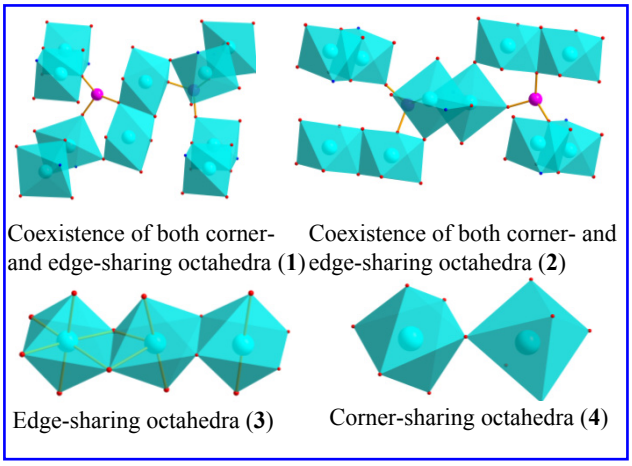

Fig. 6 Polyhedral models of corner- and edge-sharing octahedral cobalt in **1-4**. All metal centers are octahedrally coordinated. Co, O, P, and N are shown as Cyan, red, magenta, blue, respectively.

These observations suggest that μ-oxo bridging cobalt clusters are responsible for the high activity of **1** toward water oxidation. The photocatalytic mechanism of **1** can be expected to be similar to that proposed for Co-Pi.[57] For Co-Pi, mechansistic studies suggested that the water oxidation reaction occurs *via* proton-coupled electron transfer (PCET) processes. The generation of the active intermediate Co(IV)(O) requires transfer of electron and proton from Co(III)-OH metal center before the rate-determining O_2 evolution step.[58, 59] However, the close relationship between the structure and catalytic function requires a well-defined molecular structure. To further understand the relationship between the structure and catalytic activity, we examined the crystal structure of four cobalt phosphonates. Their structural parameters including the distances of Co-Co, and the Co-O and Co-N bond lengths were summarized in Table 1. As shown in Fig. 6, **1** and **2** possess corner-sharing (mono-μ-oxo bridging) and edge-sharing (di-μ-oxo bridging) octahedra. Compound **3** is composed of di-μ-oxo bridging (edge-sharing CoO_6) octahedral cobalt trinuclear cluster. Compound **4** is a mononuclear cobalt phosphonate, in which the octahedral cobalt is corner-sharing by phosphonate oxygen atoms. Such structural difference together with the catalytic performances indicates the presence of extensive di-μ-oxo bridging and mono-μ-oxo bridging octahedra could be the structural motif for highly active **1** and **2**. Compound **4** possessing mono-μ-oxo bridging octahedra without di-μ-oxo bridging was shown with low activity. Recent reports reveal that such di-μ-oxo bridges allow for the oxygen ligands to be involved in PCET[60] and are regarded as the critical structural motif for the cobalt or manganese-based water oxidation catalyst.[31, 47, 61, 62] Furthermore, a mechanistic study of oxygen evolution on Co_3O_4 nanoparticles by time-resolved FT-IR

spectroscopy also further supports that the oxo-bridged cobalt centres play a significant role in improving the photocatalytic efficiency.[63]

Thus, within the compounds possessing the edge-sharing CoO_6 octahedral cobalt, it was found that the oxygen evolution rate and oxygen yield follow a similar trend with the Co-Co distances. The longer Co-Co distances over edge-sharing (di-μ-oxo bridging) octahedra suggest that the corresponding Co-O bonds are relatively weak.[61] Interestingly, the distance of Co-N bond (2.164-2.256 Å) in **1** and **2** is significantly longer than its average bond length (2.113-2.122 Å), resulting in a distorted coordination geometry. This indicates that their structure is relatively flexible, which contributes to stabilizing the reactive intermediate. To describe the distorted geometry in more detail, we calculated their standard deviations (Table S4†). It is shown that the compound with the highly distorted structure displays better catalytic activity. Furthermore, the average bond lengths also follow the same trend (Table 1). This could partly explain why N-doping hybrids display superior catalytic activity, compared to that without N doping.[36]

Conclusions

In summary, we for the first time demonstrate a new organic cobalt phosphonate crystal as a promising heterogeneous catalyst for photocatalytic water oxidation using $[Ru(bpy)_3]Cl_2$ as the photosensitizer and $Na_2S_2O_8$ as the sacrificial oxidant in an aqueous borate buffer solution under visible light ($\lambda > 420$ nm). By the exploration of a series of cobalt phosphonates with different structures, we investigated the interplay between the structure and the catalytic activity by means of lattice parameters. On the basis of single-crystal structural analysis, we found that cobalt phosphonates containing corner-sharing (mono-μ-oxo bridging) and edge-sharing (di-μ-oxo bridging) octahedral cobalt possess longer average bond distance and hence display superior catalytic activity. The Co-N bonds play a significant role in lowering the symmetry of octahedral cobalt, resulting in a flexible and weak metal-oxygen bond. This study demonstrates that the well-defined crystal structures of the hybrid materials could pave a way for better understanding of structure-activity correlations. These findings will help us design and synthesize stable and efficient catalysts for water oxidation.

Acknowledgements

This research project is funded by the National Research Foundation (NRF), Prime Minister's Office, Singapore under its Campus for Research Excellence and Technological Enterprise (CREATE) programme: the Singapore-Berkeley Research Initiative for Sustainable Energy (SinBeRISE); and the Natural Science Foundation of Fujian Province, China (No. 2013J01065). The authors greatly thank Prof. B Liu and Dr. HB Yang for assistance in electrochemical analysis, Prof. H. W. Duan and Dr. F. Zheng for photoluminescence experiment, and Prof. R Webster for insightful discussion.

Notes and references

[a]*School of Chemical & Biomedical Engineering, Nanyang Technological University, 62 Nanyang Drive, Singapore 637459; E-ail:rxu@ntu.edu.sg*

[b]*SinBeRISE CREATE, National Research Foundation, CREATE Tower level 11, 1 Create Way, Singapore 138602; E-mail:rxu@ntu.edu.sg*

[c]*State Key Laboratory of Structural Chemistry, Fujian Institute of Research on the Structure of Matter, the Chinese Academyof Sciences, Fuzhou 350002, P. R. China; E-mail:mjg@fjirsm.ac.cn.*

[d]*School of Materials Science and Engineering. Nanyang Technological University, 50 Nanyang Avenue, 639798, Singapore*

† Electronic Supplementary Information (ESI) available: Experimental procedures, X-ray crystallography, additional Figures, characterization, properties of **1**-**4** and Co_3O_4. Crystal data for **1** is available free of charge from the Cambridge Crystallographic Data Centre under reference numbers CCDC 983193. See DOI: 10.1039/b000000x/

1. J. P. McEvoy and G. W. Brudvig, *Chem. Rev.*, 2006, 106, 4455-4483.
2. Y. Umena, K. Kawakami, J.-R. Shen and N. Kamiya, *Nature*, 2011, 473, 55-60.
3. Y. Tachibana, L. Vayssieres and J. R. Durrant, *Nat Photon*, 2012, 6, 511-518.
4. R. Liu, G. Yuan, C. L. Joe, T. E. Lightburn, K. L. Tan and D. Wang, *Angew Chem, Int Ed*, 2012, 51, 6709-6712.
5. D. G. Nocera, *Acc. Chem. Res.*, 2012, 45, 767-776.
6. K. Kalyanasundaram and M. Graetzel, *Curr. Opin. Biotechnol.*, 2010, 21, 298-310.
7. A. Singh and L. Spiccia, *Coord. Chem. Rev.*, 2013, 257, 2607-2622.
8. J. Limburg, J. S. Vrettos, L. M. Liable-Sands, A. L. Rheingold, R. H. Crabtree and G. W. Brudvig, *Science*, 1999, 283, 1524-1527.
9. V. Artero, M. Chavarot-Kerlidou and M. Fontecave, *Angew. Chem. Int. Ed.*, 2011, 50, 7238-7266.
10. M.-R. Gao, Y.-F. Xu, J. Jiang, Y.-R. Zheng and S.-H. Yu, *J. Am. Chem. Soc.*, 2012, 134, 2930-2933.
11. H. S. Ahn and T. D. Tilley, *Adv. Funct. Mater.*, 2013, 23, 227-233.
12. J. B. Gerken, J. G. McAlpin, J. Y. C. Chen, M. L. Rigsby, W. H. Casey, R. D. Britt and S. S. Stahl, *J. Am. Chem. Soc.*, 2011, 133, 14431-14442.
13. F. Jiao and H. Frei, *Energy Environ. Sci*, 2010, 3, 1018-1027.
14. N. S. McCool, D. M. Robinson, J. E. Sheats and G. C. Dismukes, *J. Am. Chem. Soc.*, 2011, 133, 11446-11449.
15. S. Berardi, G. La Ganga, M. Natali, I. Bazzan, F. Puntoriero, A. Sartorel, F. Scandola, S. Campagna and M. Bonchio, *J. Am. Chem. Soc.*, 2012, 134, 11104-11107.
16. M. D. Symes, D. A. Lutterman, T. S. Teets, B. L. Anderson, J. J. Breen and D. G. Nocera, *ChemSusChem*, 2013, 6, 65-69.
17. F. Evangelisti, R. Güttinger, R. Moré, S. Luber and G. R. Patzke, *J. Am. Chem. Soc.*, 2013, 135, 18734-18737.
18. Q. Yin, J. M. Tan, C. Besson, Y. V. Geletii, D. G. Musaev, A. E. Kuznetsov, Z. Luo, K. I. Hardcastle and C. L. Hill, *Science*, 2010, 328, 342-345.
19. Z. Huang, Z. Luo, Y. V. Geletii, J. W. Vickers, Q. Yin, D. Wu, Y. Hou, Y. Ding, J. Song, D. G. Musaev, C. L. Hill and T. Lian, *J. Am. Chem. Soc.*, 2011, 133, 2068-2071.
20. J. W. Vickers, H. Lv, J. M. Sumliner, G. Zhu, Z. Luo, D. G. Musaev, Y. V. Geletii and C. L. Hill, *J. Am. Chem. Soc.*, 2013, 135, 14110-14118.
21. F. Jiao and H. Frei, *Angew. Chem. Int. Ed.*, 2009, 48, 1841-1844.
22. G. P. Gardner, Y. B. Go, D. M. Robinson, P. F. Smith, J. Hadermann, A. Abakumov, M. Greenblatt and G. C. Dismukes, *Angew Chem, Int Ed*, 2012, 51, 1616-1619.
23. J. Suntivich, K. J. May, H. A. Gasteiger, J. B. Goodenough and Y. Shao-Horn, *Science*, 2011, 334, 1383-1385.
24. Y. Yamada, K. Yano, D. Hong and S. Fukuzumi, *Phys. Chem. Chem. Phys.*, 2012, 14, 5753-5760.
25. S. Pintado, S. Goberna-Ferrón, E. C. Escudero-Adán and J. R. Galán-Mascarós, *J. Am. Chem. Soc.*, 2013, 135, 13270-13273.
26. M. W. Kanan and D. G. Nocera, *Science*, 2008, 321, 1072-1075.
27. M. Risch, V. Khare, I. Zaharieva, L. Gerencser, P. Chernev and H. Dau, *J. Am. Chem. Soc.*, 2009, 131, 6936-6937.
28. X. L. Hu, S. Piccinin, A. Laio and S. Fabris, *ACS Nano*, 2012, 6, 10497-10504.
29. D. Shevchenko, M. F. Anderlund, A. Thapper and S. Styring, *Energy Environ. Sci.*, 2011, 4, 1284-1287.

30. M. Risch, D. Shevchenko, M. F. Anderlund, S. Styring, J. Heidkamp, K. M. Lange, A. Thapper and I. Zaharieva, *Int. J. Hydrogen Energy*, 2012, 37, 8878-8888.
31. K. Jin, J. Park, J. Lee, K. D. Yang, G. K. Pradhan, U. Sim, D. Jeong, H. L. Jang, S. Park, D. Kim, N.-E. Sung, S. H. Kim, S. Han and K. T. Nam, *J. Am. Chem. Soc.*, 2014, 136, 7435-7443.
32. Y. V. Geletii, Z. Huang, Y. Hou, D. G. Musaev, T. Lian and C. L. Hill, *J. Am. Chem. Soc.*, 2009, 131, 7522-7523.
33. D. Hong, Y. Yamada, T. Nagatomi, Y. Takai and S. Fukuzumi, *J. Am. Chem. Soc.*, 2012, 134, 19572-19575.
34. M. Grzelczak, J. Zhang, J. Pfrommer, J. Hartmann, M. Driess, M. Antonietti and X. Wang, *ACS Catal*, 2013, 3, 383-388.
35. H. S. Ahn, J. Yano and T. D. Tilley, *Energy Environ. Sci*, 2013, 6, 3080-3087.
36. Y. Liang, Y. Li, H. Wang, J. Zhou, J. Wang, T. Regier and H. Dai, *Nat. Mater.*, 2011, 10, 780-786.
37. A. Vaidyalingam and P. K. Dutta, *Anal. Chem.*, 2000, 72, 5219-5224.
38. H. Lv, J. Song, Y. V. Geletii, J. W. Vickers, J. M. Sumliner, D. G. Musaev, P. Kögerler, P. F. Zhuk, J. Bacsa, G. Zhu and C. L. Hill, *J. Am. Chem. Soc.*, 2014, 136, 9268-9271.
39. X.-B. Han, Z.-M. Zhang, T. Zhang, Y.-G. Li, W. Lin, W. You, Z.-M. Su and E.-B. Wang, *J. Am. Chem. Soc.*, 2014, 136, 5359-5366.
40. F. Song, Y. Ding, B. Ma, C. Wang, Q. Wang, X. Du, S. Fu and J. Song, *Energy Environ. Sci.*, 2013, 6, 1170-1184.
41. A. Harriman, I. J. Pickering, J. M. Thomas and P. A. Christensen, *J. Chem. Soc., Faraday Trans.*, 1988, 84, 2795-2806.
42. A. Lewandowska-Andralojc and D. E. Polyansky, *J. Phys. Chem. A*, 2013, 117, 10311-10319.
43. D. Hong, J. Jung, J. Park, Y. Yamada, T. Suenobu, Y.-M. Lee, W. Nam and S. Fukuzumi, *Energy Environ. Sci*, 2012, 5, 7606-7616.
44. Z. Huang, Y. V. Geletii, D. G. Musaev, C. L. Hill and T. Lian, *Ind. Eng. Chem. Res.*, 2012, 51, 11850-11859.
45. A. Lewandowska-Andralojc, D. E. Polyansky, R. Zong, R. P. Thummel and E. Fujita, *Phys. Chem. Chem. Phys.*, 2013, 15, 14058-14068.
46. M. Hara, C. C. Waraksa, J. T. Lean, B. A. Lewis and T. E. Mallouk, *J. Phys. Chem. A*, 2000, 104, 5275-5280.
47. M. W. Kanan, J. Yano, Y. Surendranath, M. Dincă, V. K. Yachandra and D. G. Nocera, *J. Am. Chem. Soc.*, 2010, 132, 13692-13701.
48. S. W. Lee, C. Carlton, M. Risch, Y. Surendranath, S. Chen, S. Furutsuki, A. Yamada, D. G. Nocera and Y. Shao-Horn, *J. Am. Chem. Soc.*, 2012, 134, 16959-16962.
49. M. D. Kärkäs, O. Verho, E. V. Johnston and B. Åkermark, *Chem. Rev.* 2014, DOI: 10.1021/cr400572f.
50. M. Natali, S. Berardi, A. Sartorel, M. Bonchio, S. Campagna and F. Scandola, *Chem. Commun.*, 2012, 48, 8808-8810.
51. D. K. Bediako, Y. Surendranath and D. G. Nocera, *J. Am. Chem. Soc.*, 2013, 135, 3662-3674.
52. T. Nakagawa, C. A. Beasley and R. W. Murray, *J. Phys. Chem. C*, 2009, 113, 12958-12961.
53. S.-X. Guo, Y. Liu, C.-Y. Lee, A. M. Bond, J. Zhang, Y. V. Geletii and C. L. Hill, *Energy Environ. Sci*, 2013, 6, 2654-2663.
54. T. W. Kim, M. A. Woo, M. Regis and K.-S. Choi, *J. Phys. Chem. Lett.*, 2014, 5, 2370-2374.
55. Y. Surendranath, M. W. Kanan and D. G. Nocera, *J. Am. Chem. Soc.*, 2010, 132, 16501-16509.
56. S. Yusuf and F. Jiao, *ACS. Catal.*, 2012, 2, 2753-2760.
57. Y. Surendranath, D. A. Lutterman, Y. Liu and D. G. Nocera, *J. Am. Chem. Soc.*, 2012, 134, 6326-6336.
58. D. K. Dogutan, R. McGuire and D. G. Nocera, *J. Am. Chem. Soc.*, 2011, 133, 9178-9180.
59. C. A. Kent, J. J. Concepcion, C. J. Dares, D. A. Torelli, A. J. Rieth, A. S. Miller, P. G. Hoertz and T. J. Meyer, *J. Am. Chem. Soc.*, 2013, 135, 8432-8435.
60. P. E. M. Siegbahn, *Acc. Chem. Res.*, 2009, 42, 1871-1880.
61. D. M. Robinson, Y. B. Go, M. Mui, G. Gardner, Z. Zhang, D. Mastrogiovanni, E. Garfunkel, J. Li, M. Greenblatt and G. C. Dismukes, *J. Am. Chem. Soc.*, 2013, 135, 3494-3501.
62. A. Bergmann, I. Zaharieva, H. Dau and P. Strasser, *Energy Environ. Sci*, 2013, 6, 2745-2755.
63. M. Zhang, M. de Respinis and H. Frei, *Nat Chem*, 2014, 6, 362-367.

Graphical Abstracts

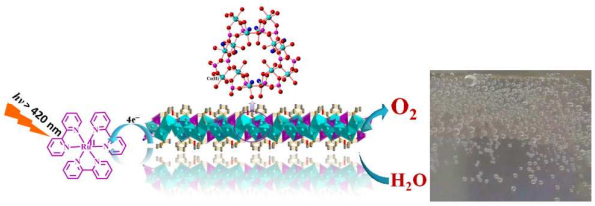

A new layered metal-organic phosphonate crystal with both mono-and di-μ-oxo bridged octahedral cobalt was synthesized and acts as an efficient and stable heterogeneous catalyst for water oxidation.

Supplementary Materials

Bio-inspired organic cobalt(II) phosphonates toward water oxidation

*Tianhua Zhou, Danping Wang, Simon Chun-Kiat Goh, Jindui Hong, Jianyu Han, Jianggao Mao*and Rong Xu**

Material

All solvents and chemicals are obtained from commercial supplies and used directly as received unless otherwise stated. [Ru(2,2'-bipyridine)$_3$]Cl$_2$, 3-phosphonopropionic acid (PPAH$_3$), phenylphosphonic acid (PPH$_3$) and sodium tetraboratedecahydrate were purchased from Sigma-Aldrich. $Na_2S_2O_8$ was obtained from Alfa Aesar.$^{18}OH_2$ solution (97%) was purchased from Cambridge Isotopes Labs. *N*-(phosphonomethyl)proline (S-H$_3$L)[S1] were prepared according to the procedures in our previous reports. Co_3O_4 nanocrystals were synthesized according to the reported method.[S2,S3]

Methods

Characterization

Elemental analysis (C, H, N) was performed on an Elementary Vario El III instrument. FT-IR spectra were obtained with a Perkin Elmer FT-IR Spectrum GX using KBr technique in the range of 4000–400 cm^{-1}. Thermogravimetric analyses (TGA) were carried out with a TA Intruments TGA 5000 instrument at a heating rate of 15 °C/min under air atmosphere. Powder X-ray diffraction (XRD) patterns were obtained on a Bruker AXS D2 Advanced X-ray diffractometer with monochromatized Cu Ka radiation (λ = 1.54056 Å, 40 kV and 20 mA). The data were collected with 2θ in a range of 5°-65° and a step size of 0.02°/0.5 s. All measurements were performed at room temperature and atmospheric pressure. UV-Vis diffuse reflectance spectra (DRS) were obtained by UV-visible absorption spectroscopy (UV-2450,

Shimadzu). The chemical state of cobalt was analyzed by means of XPS analysis performed on a VG Escalab 220iXL and the binding energies were calibrated using the C 1s peak at 285.0 eV. TEM was performed on transmission electron microscopy (TEM, JEOL JEM-3010 and JEM-2100). BET surface areas of both as-synthesized crystal samples (without grinding) and grinded samples were measured by N_2 adsorption and desorption at 77 K using a Quantachrome Autosorb-6 sorption system. Samples were degassed offline at 100 °C or 80 °C for 20 h under vacuum before the analysis. Inductively coupled plasma mass spectrometry was performed with an Agilent 7700x-MS Inductively Coupled Plasma-Mass Spectrometer (ICP-MS). Samples were prepared as described for photocatalytic water oxidation. The solid samples were removed from the solution with 20 min of centrifugation at 20,000 rpm after visible-light irradiation for 80 min. The remaining solution was used for analysis.

Fluorescence spectra

Fluorescence spectra of 1 mM $[Ru(2,2'\text{-bipyridine})_3]Cl_2$ dissolved in 40 mM borate buffer (pH 9.0) in the absence and presence of 5 mM $Na_2S_2O_8$ were collected on a Fluoromax-3 spectrometer (Horiba Scientific). The latter solution was further added with the catalyst (**1** and Co_3O_4, 0.14 g L^{-1}) for fluorescence study.

Electrochemistry

The electrochemical measurements were carried out on a CHI660C electrochemical workstation (CH Instruments, Shanghai Chenghua Co.) with a conventional three-electrode cell consisting of a Pt plate as the counter electrode. The Ag/AgCl (3 M KCl filled) was used as the reference electrode. Electrochemical data were adjusted to NHE by adding 0.197 V to the potential measurements. Solutions of 0.1 M electrolyte were prepared by mixing appropriate volumes of 0.1 M KH_2PO_4 and 0.1 M K_2HPO_4

and the pH of the solution was adjusted to desired values by titrating with 0.1 M HNO_3 or KOH aqueous solution. The pH was measured with a digital pH meter (Sartorius DOCU). The working electrode was prepared as following. A glassy carbon electrode was polished with 0.05μm Al_2O_3.Then the electrode was ultrasonicated in deionized water, ethanol and acetone, followed by drying at room temperature. An appropriate weight of cobalt phosphonates (5 mg) was dispersed in a mixture of 16 μL of 5 wt% Naphthol ethanol solution, 250 μL of 2-propanol and 750 μL of water followed by homogenization using a ultrasonication. Then 10 μL of the catalyst suspension was loaded on a glassy carbon electrode of 5 mm rotating disk electrode (RDE) (loading about 0.25 mg cm^{-2}) and dried in air at room temperature. Prior to measurement, the electrolyte was thoroughly bubbled by purging it with oxygen. Then the RDE was subjected to potential cycling (0.4 to 1.54 V vs NHE, 100 mV/s) in 0.1 M phosphate buffer solution (pH 7) at least 40 cycles before cyclic voltammetry (CV) were recorded at a scan rate of 20 mV/s with rotating rate of 1600 rpm. Linear sweep voltammetry (LSV) was obtained with a scan rate of 2 mV/s, which was also used to collect the Tafel data. The resistance collected was used to correct the Tafel plot for iR drop. Overpotential η was calculated by (V_{meas} – iR) – E (pH7.0) (where V_{meas} is the measured potential). To investigate the stability of all the samples, CV was repeated using a scan rate of 100 mV/s from 0.4 V to 1.5 V in 0.1 M phosphate buffer solution, after that LSV was recorded at a scan rate of 2 mV/s. Steady-state currents were collected at a variety of applied potentials starting at 1.2 V and proceeding in 10-20 mV steps to 0.98 V with rotating rate of 1600 rpm. The resistance collected was used to correct the Tafel plot for iR drop. The electrochemical measurements were also carried out in 0.04 M borate buffer solution (pH 9.0) according to the procedure above in phosphate buffer solution.

Single-Crystal Structure Determination

Single-crystal X-ray diffraction analyse was performed on a Rigaku Mercury CCD diffractometer (**1**). The diffractometer was equipped with graphite-monochromated Mo Kα radiation (λ = 0.7107 Å).

Intensity data were collected by the narrow-frame method at 293 K. The data sets were corrected for Lorentz and polarization factors as well as for absorption by the multi-scan method.[S4] Structure was solved by direct methods and refined by full-matrix least-squares fitting on F^2 by SHELX-97.[S5] All non-hydrogen atoms were refined with anisotropic thermal parameters. All hydrogen atoms bonded to carbon and nitrogen atoms were located at geometrically calculated positions and refined with isotropic thermal parameters. The details of crystallographic data and selected bond lengths for the two compounds are summarized in Tables S1and S2.

Synthesis of Compound 1

Compound **1** was synthesized as follows: a mixture of $Co(NO_3)_2 \cdot 6H_2O$ (0.179 g, 0.6 mmol), S-H_3L (0.100 g, 0.48 mmol), and 2,2'-bipyridine (0.032 g, 0.20 mmol) in 5 mL of deionized water, added with five drops of $(CH_3)_4NOH$, was sealed in a 23-mL Teflon-lined stainless steel autoclave, followed by heating at 170 °C for 120 h. The autoclave was then slowly cooled to room temperature. Pink plate crystals of S-H_3L-Co suitable for single-crystal X-ray diffraction analysis were isolated from the final reaction mixture by filtration, washed several times with deionized water, and dried in air at ambient temperature. Yield: 11% based on S-H_3L. The purity of the sample was confirmed by powder XRD and elemental analyses. Anal.Calcd for$C_{12}H_{26}N_2O_{14}P_2Co_3$: C, 21.80; H, 3.96; N, 4.24. Found: C, 21.22; H, 4.12; N, 4.48.

Synthesis of Compound 2

Compound **2** was synthesized according to the modified literature method.[S6] Briefly, $Co(NO_3)_2 \cdot 6H_2O$ (0.179 g, 0.6 mmol) and S-H_3L (0.100 g, 0.48 mmol) were added in 10 mL of deionized water which was further added with 0.5 mL of $(C_4H_9)_4NOH$. The mixture was then transferred into a 23-mL Teflon-lined stainless steel autoclave which was heated at 170 °C for 120 h. After the autoclave was cooled to room temperature, pink plate crystals were isolated from the final reaction mixture by filtration, washed

several times with deionized water and dried in air at ambient temperature. Yield: 13% based on S-H_3L. Anal.Calcd for$C_{12}H_{28}N_2O_{15}P_2Co_3$: C, 21.22; H, 4.16; N, 4.13. Found: C, 20.85; H, 4.23; N,4.27.

Synthesis of Compound 3

Compound **3** was synthesized according to the modified literature method.[S7] A mixture of $Co(CH_3COO)_2{\cdot}4H_2O$ (0.455 g, 1.83mmol) and $PPAH_3$ (0.289 g, 1.83 mmol) in 10 mL of deionized water was sealed in a 23-mL Teflon-lined stainless steel autoclave followed by heating at 120 °C for 72 h. The autoclave was then slowly cooled to room temperature. Pink spherical crystals of PPA-Co were isolated from the final reaction mixture by filtration, washed several times with deionized water, and dried in air at ambient temperature. Yield: 11% based on $Co(CH_3COO)_2{\cdot}4H_2O$. Anal. Calcd for $C_6H_{20}O_{16}P_2Co_3$: C, 12.28; H, 3.43. Found: C, 12.50; O, 2.81.

Synthesis of Compound 4

Compound **4** was synthesized according to the modified literature method.[S8] A mixture of $CoCl_2$ (0.0713 g, 0.5 mmol) and PPH_3 (0.047 g, 0.3 mmol) in 10 mL of water, with three drops of $(CH_3)_4NOH$ added, was sealed in a 23-mL Teflon-lined stainless steel autoclave at 140 °C for 72 h. The autoclave was then slowly cooled to room temperature. Pink plate crystals of PP-Co were isolated from the final reaction mixture by filtration, washed several times with distilled water, and dried in air at ambient temperature. Yield: 11% based on S-H_3L. Anal. Calcd for $C_6H_7O_4PCo$: C, 30.93; H, 3.03. Found: C, 31.02; O, 2.916. In addition, **4** can also be synthesized using a mixture of $Co(CH_3COO)_2{\cdot}4H_2O$ (0.455 g, 1.83 mmol) and PPH_3 (0.295 g, 1.83 mmol) dissolved in 10 mL of water. After stirring for 10 min and sealed in 23-mL Teflon-lined stainless steel autoclave at 140 °C for 48 h, polycrystalline pure phase was obtained after cooling to room temperature.

Table S1. Summary of crystal data and structural refinements for **1.**

Compound	**1**
Formula	$C_{12}H_{26}N_2O_{14}P_2Co_3$
Fw	661.08
Crystal system	Monoclinic
Space group	*C*2/*c*
a (Å)	23.446(10)
b (Å)	9.956(4)
c (Å)	19.018(8)
β(°)	98.983(5)
V (Å^3)	4385(3)
Z	8
D_{calcd}(g·cm^{-3})	2.003
F(000)	2680
μ(mm^{-1})	2.463
R_1, wR_2 [$I>2\sigma(I)$][a]	0.0462, 0.0939
R_1, wR_2 (all data)[a]	0.0647, 0.1047

[a] $R_1 = \Sigma||F_o| - |F_c||/\Sigma|F_o|$, $wR_2 = \{\Sigma w[(F_o)^2 - (F_c)^2]^2/\Sigma w[(F_o)^2]^2\}^{1/2}$.

Table S2. Selected bond length (Å) for **1**.[a]

1			
Co(1)-O(8)#1	2.006(3)	Co(3)-O(6)#1	2.149(3)
Co(1)-O(2)#2	2.089(3)	Co(3)-O(4W)	2.191(3)
Co(1)-O(5)	2.108(3)	Co(3)-O(5)	2.199(3)
Co(1)-O(2W)	2.155(3)	O(4)-C(6)	1.250(4)
Co(1)-O(2)	2.165(3)	O(5)-C(6)	1.269(4)
Co(1)-N(1)	2.209(3)	O(9)-C(12)	1.257(6)
Co(2)-O(1)	2.034(3)	O(10)-C(12)	1.257(5)
Co(2)-O(10)	2.059(3)	P(1)-O(1)	1.511(3)
Co(2)-O(7)	2.090(3)	P(1)-O(3)	1.512(3)
Co(2)-O(7)#3	2.120(3)	P(1)-O(2)	1.543(3)
Co(2)-O(1W)	2.142(3)	P(1)-C(5)	1.813(3)
Co(2)-N(2)	2.256(4)	P(2)-O(8)	1.505(3)
Co(3)-O(3)#2	2.028(3)	P(2)-O(6)	1.527(3)
Co(3)-O(3W)	2.082(3)	P(2)-O(7)	1.531(3)
Co(3)-O(6)#4	2.119(3)	P(2)-C(11)	1.820(4)

[a] Symmetry code to generate equivalent atoms:#1 x,-y+1,z+1/2; #2 -x+1,y,-z+1/2; #3 -x+1,-y+1,-z; #4 -x+1,y-1,-z+1/2.

Table S3. Hydrogen bond distances (Å) and angles (º) for **1**.

D-H...A	d(D-H)	d(H...A)	d(D...A)	<(DHA)
O(1W)-(1WB)...O(4W)#5	0.85	1.87	2.715(4)	173.8
O(2W)-H(2WA)...O(9)#1	0.85	1.88	2.725(5)	178.8
O(4W)-H(4WB)...O(4)#2	0.85	2.01	2.844(5)	165.7

Symmetry transformations used to generate equivalent atoms:
#1 x,-y+1,z+1/2; #2 -x+1,y,-z-1/2; #5 -x+1,y+1,-z-1/2.

Table S4. Water oxidation activities of cobalt phosphonate catalysts.

Catalyst	TOF × 10^3 (s^{-1})[a]	TOF (μmol s^{-1} m^{-2})[b]	TON[c]	Yield (%)[d]	BET (m^2 g^{-1})	Bond length standard deviation(δ)[e]
1	5.16±0.02	0.30±0.02	10±2	78±2	23	0.0659
2	3.81±0.02	0.29±0.02	9±2	77±2	20	0.0573
3	3.21±0.03	0.19±0.03	6±1	57±2	26	0.0524
4	0.89±0.03	0.05±0.03	2±1	40±1	81	0.0778
Co_3O_4	0.51±0.03	0.03±2	1	21±1	74	
Co_3O_4[e]	1.14[f]	0.14[f]		64[f]	34[f]	

[a]Turnover frequency defined as O_2 evolution rates after 10 min of photo-irradiation/catalyst amount.

[b]Apparent turnover frequency defined as O_2 evolution rates after 10 min of photoirradiation/catalyst weight/specific surface area.

[c]TON defined as the amount of oxygen evolved/the amount of catalyst.

[d]Yield = (mole of O_2)/(1/2×mol of $Na_2S_2O_8$).

[e] $\delta = \sqrt{\frac{\sum(l_i - l_0)^2}{i}}$, l_i, referred to as Co-X(X = O, or/and N) distances; l_0, averaged Co-X(X = O,N)bond distance. i, the total amount of Co-X(X = O,N)bond.

[f]Data from Ref S9.

Table S5. The pH values of the photocatalytic system after photocatalysis.[a]

Catalyst	pH value of borate buffer	Reaction time (min)	pH value after photocatalysis
1	9.0	80	8.63
2	9.0	80	8.65
3	9.0	80	8.64
4	9.0	80	8.57

[a]Reaction condition: 0.14 g L^{-1} catalyst, 1.0 mM $[Ru(bpy)_3]^{2+}$, 5.0 mM $Na_2S_2O_8$, 40 mM borate buffer, total volume of the reaction solution 10 mL, light source: 300 W Xe lamp with 420 nm cut-off filter.

Table S6. Water oxidation activities of as-synthesized crystal cobalt phosphonate catalysts.

Catalyst	R_{O2} (μmol s^{-1} g^{-1})[a]	TOF × 10^3 (s^{-1})[b]	TOF (μmol s^{-1} m^{-2})[c]	Yield (%)[d]	BET (m^2 g^{-1})
1	5.1±0.4	3.41±0.04	1.13±0.03	57±2	4.6
2	4.8±0.3	3.27±0.03	0.89±0.03	50±1	5.4
3	3.7±0.2	2.15±0.02	0.57±0.03	41±2	6.4
4	2.3±0.4	0.52±0.04	0.15±0.03	23±3	14.9

[a]O_2 evolution rate (normalized by the catalyst mass) after irradiation for 10 min.
[b]Turnover frequency defined as O_2 evolution rate after 10 min of photo-irradiation/catalyst amount.
[c]Apparent turnover frequency defined as O_2 evolution rates after 10 min of photoirradiation/catalyst weight/specific surface area.
[d]Yield = (mole of O_2)/(1/2×mol of $Na_2S_2O_8$).
Reaction condition: as-synthesized crystal sample (0.14 g L^{-1}), 1.0 mM $[Ru(bpy)_3]^{2+}$, 5.0 mM $Na_2S_2O_8$, 40 mM borate buffer (initial pH 9.0), total volume of the reaction solution 10 mL, light source: 300 W Xe lamp with 420 nm cut-off filter.

Table S7. ICP-MS data for solution after photocatalytic reaction.[a]

Catalyst	Cobalt phosphonates (μM)	Reaction time (min)	Cobalt in reaction solution after centrifugation (μM)	Cobalt species dissolved in reaction solution (%)
1	535	80	31	1.9
2	552	80	38	2.3
3	537	80	25	1.5
4	515	80	12	2.3

[a]Reaction condition: 0.14 g L^{-1}catalyst, 1.0 mM $[Ru(bpy)_3]^{2+}$, 5.0 mM $Na_2S_2O_8$, 40 mM borate buffer (initial pH 9.0), total volume of the reaction solution 10 mL, light source: 300 W Xe lamp with 420 nm cut-off filter.

Table S8. Electrochemical properties of cobalt phosphonate catalysts.[a]

Catalyst	100 mM phosphate buffer (pH 7)			40 mM Borate buffer (pH 9)	
	Over-potential (η, mV)	Tafel slope (mV/decade)[a]	Tafel slope (mV/decade)[b]	Over-potential (η, mV)	Tafel slope (mV/decade)[b]
1	484	83±1	92±2	468	68
2	493	83±1	94±2	474	69
3	503	85±2	94±1	494	74
4	508	90±3	96±1	497	74
Co_3O_4	481	82±5	82±2	454	66
Co_3O_4[c]	480	88			

[a] Data were calculated from LSV.
[b] Data were calculated based on steady state data.
[c] Data from Ref. S10.

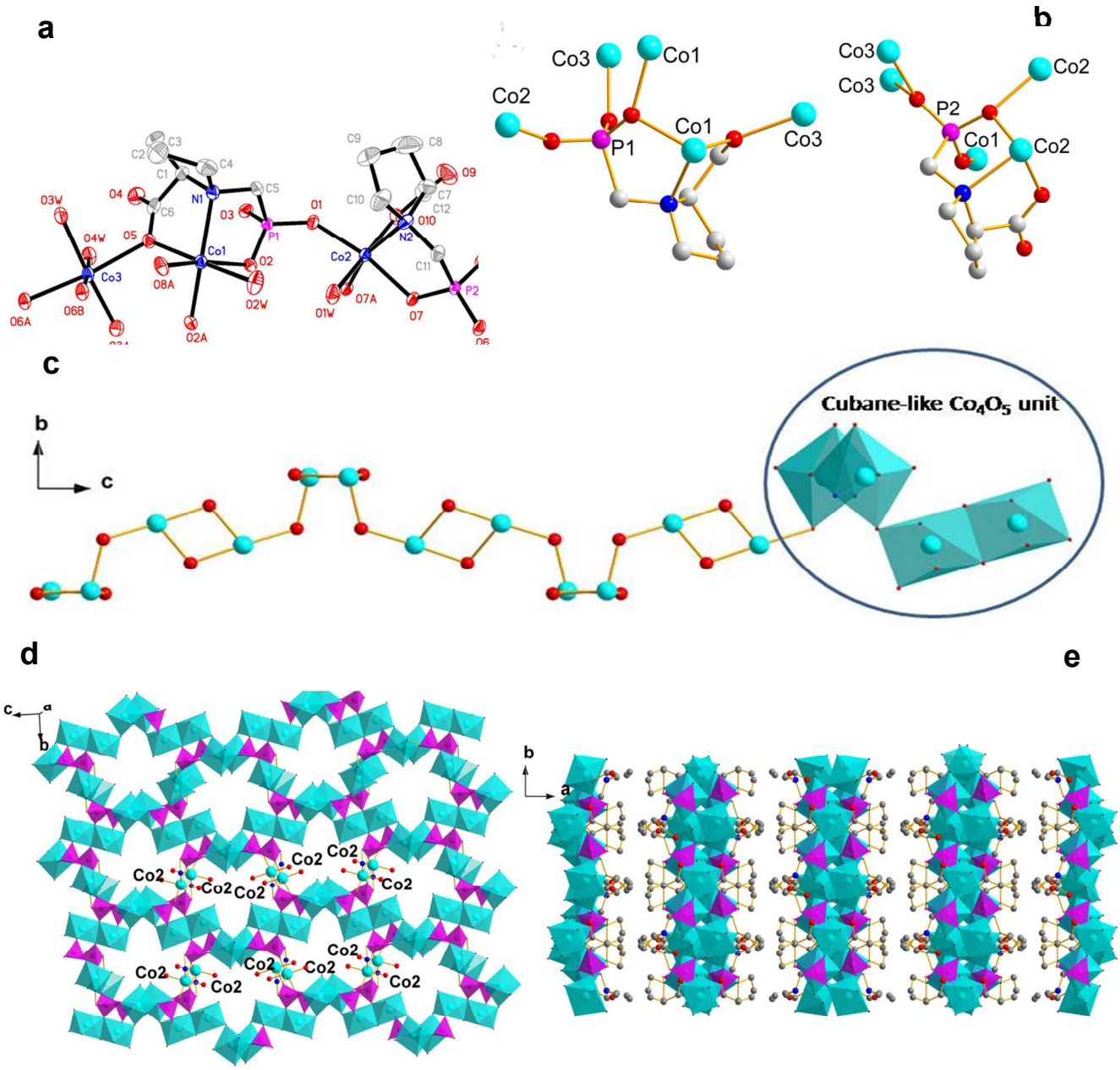

Fig. S1 (a) ORTEP drawing of the asymmetric unit in **1** with atomic labeling scheme. Thermal ellipsoids are at the 30% probability level. H atoms and lattice water molecules were omitted for clarity. (b) The coordination models of S-H_3L ligand in **1**. (c) Co-O chain consisting of cubane-like Co_4O_5 unit along the *c*-axis. (d) Inorganic layer of **1** in the *bc* plane. (e) Layered architecture of **1** along *c*-axis. Co, O, P, and N are shown as cyan, red, magenta, and blue circles, respectively. CoO_6, CoO_5N polydedra and CPO_3 tetrahedra are shaded in cyan and magenta, respectively.

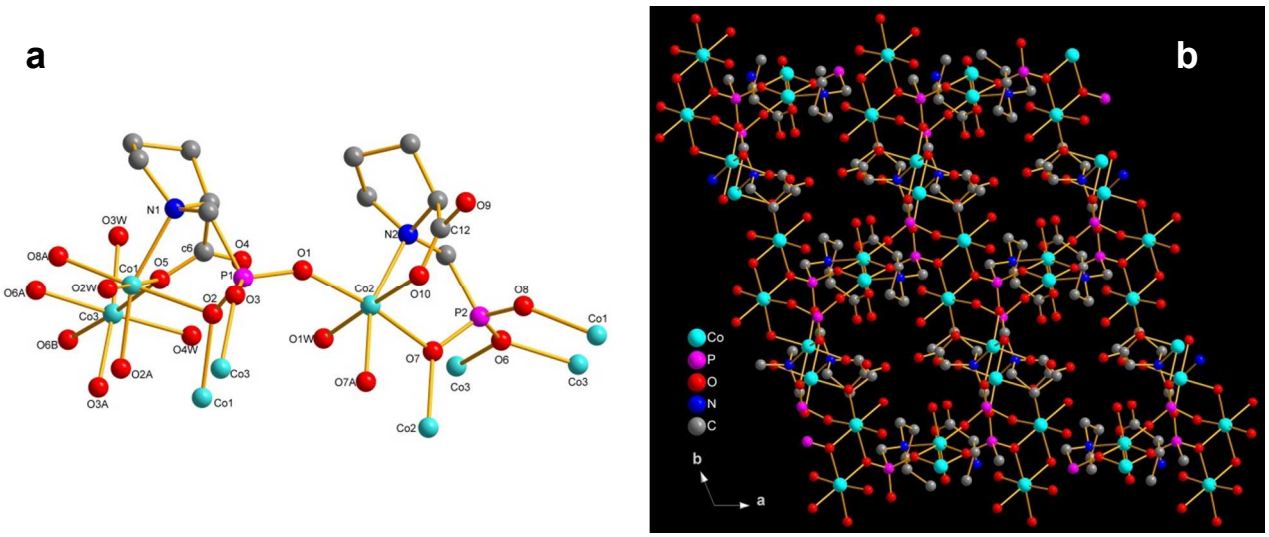

Fig. S2 (a) The coordination environment around cobalt(II) ion in **2**, and (b) crystal structural packing of **2** in the *ab* plane. CIF file was obtained from Cambridge Crystallographic *Data* Centre (*CCDC*199770).

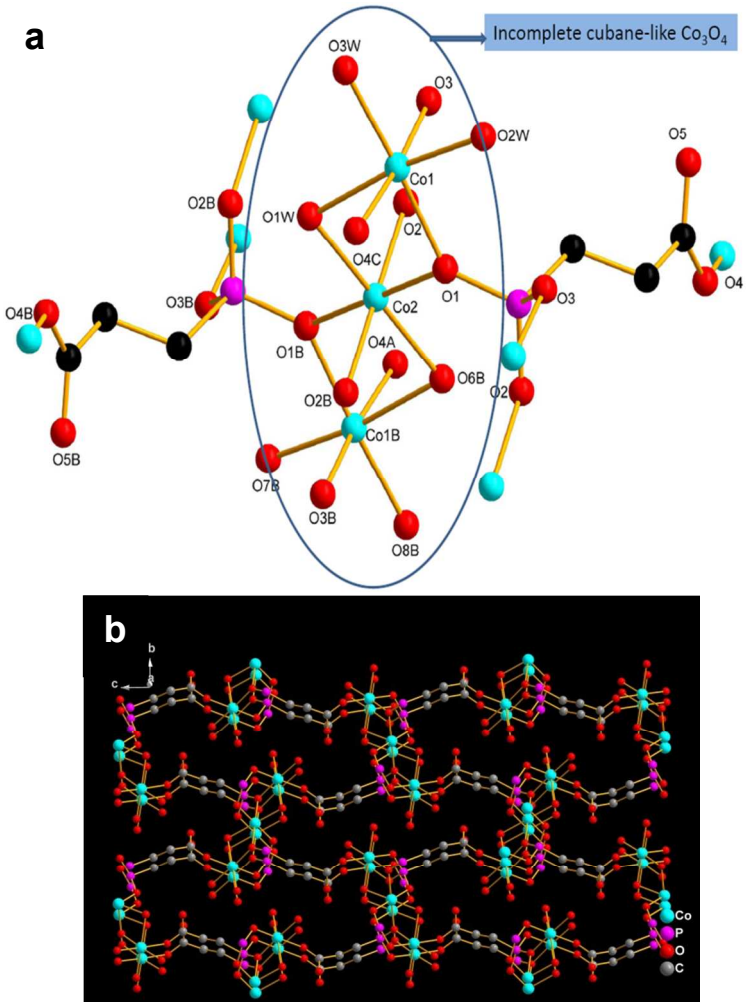

Fig. S3 (a) The coordination environment around cobalt(II) ion in **3**, and (b) crystal structural packing of **3** in the *bc* plane. CIF file was obtained from Cambridge Crystallographic *Data* Centre (WebCSD:SOMQUG).

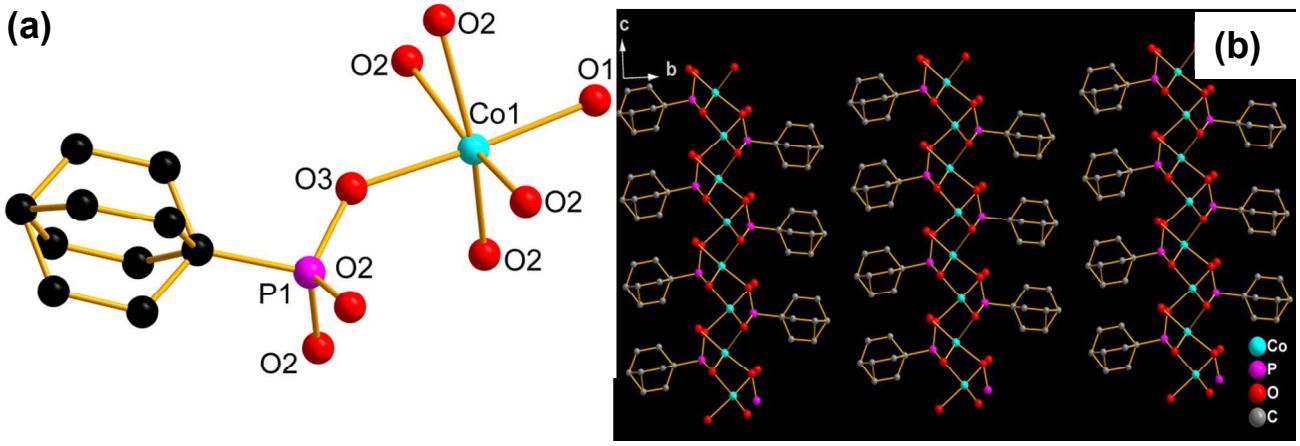

Fig. S4 (a) The coordination environment around cobalt(II) ion in **4**, and (b) Crystal structural packing of Compound **4** in the *ab* plane. CIF file was obtained from Cambridge Crystallographic Data Centre (CCDC 279873).

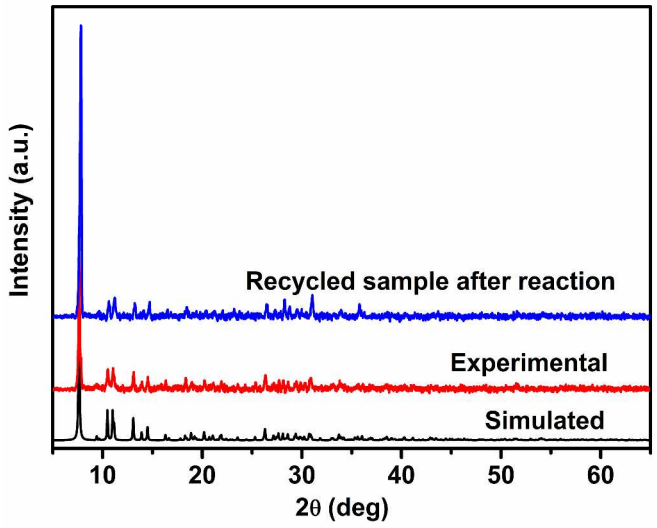

Fig. S5 Simulated and experimental XRD powder patterns for **1**.

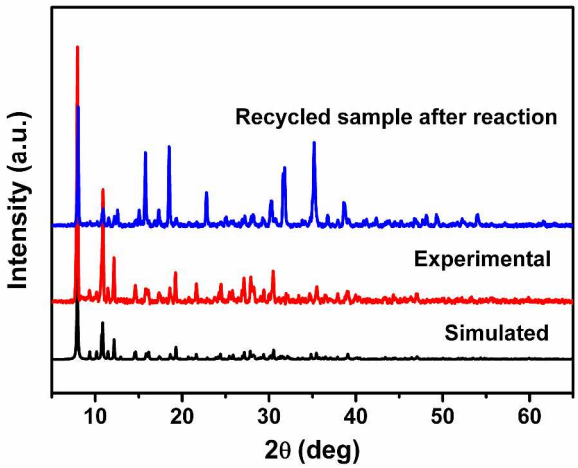

Fig. S6 Simulated and experimental XRD powder patterns for **2**.

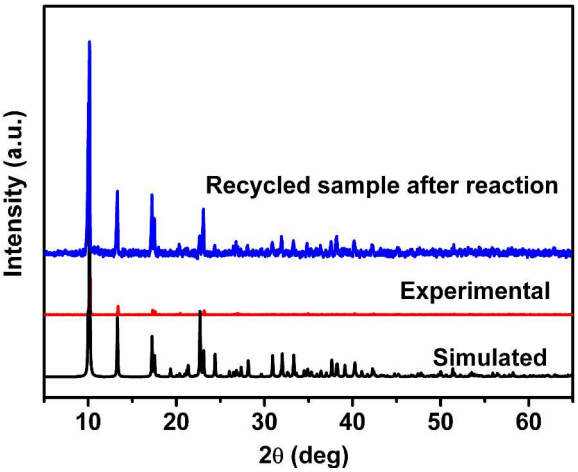

Fig. S7 Simulated and experimental XRD powder patterns for **3**.

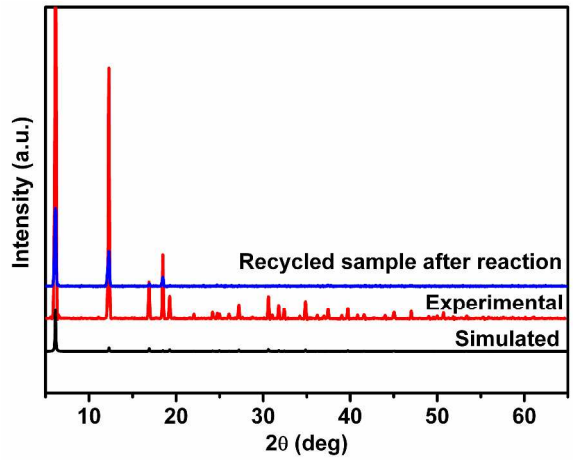

Fig. S8 Simulated and experimental XRD powder patterns for **4**.

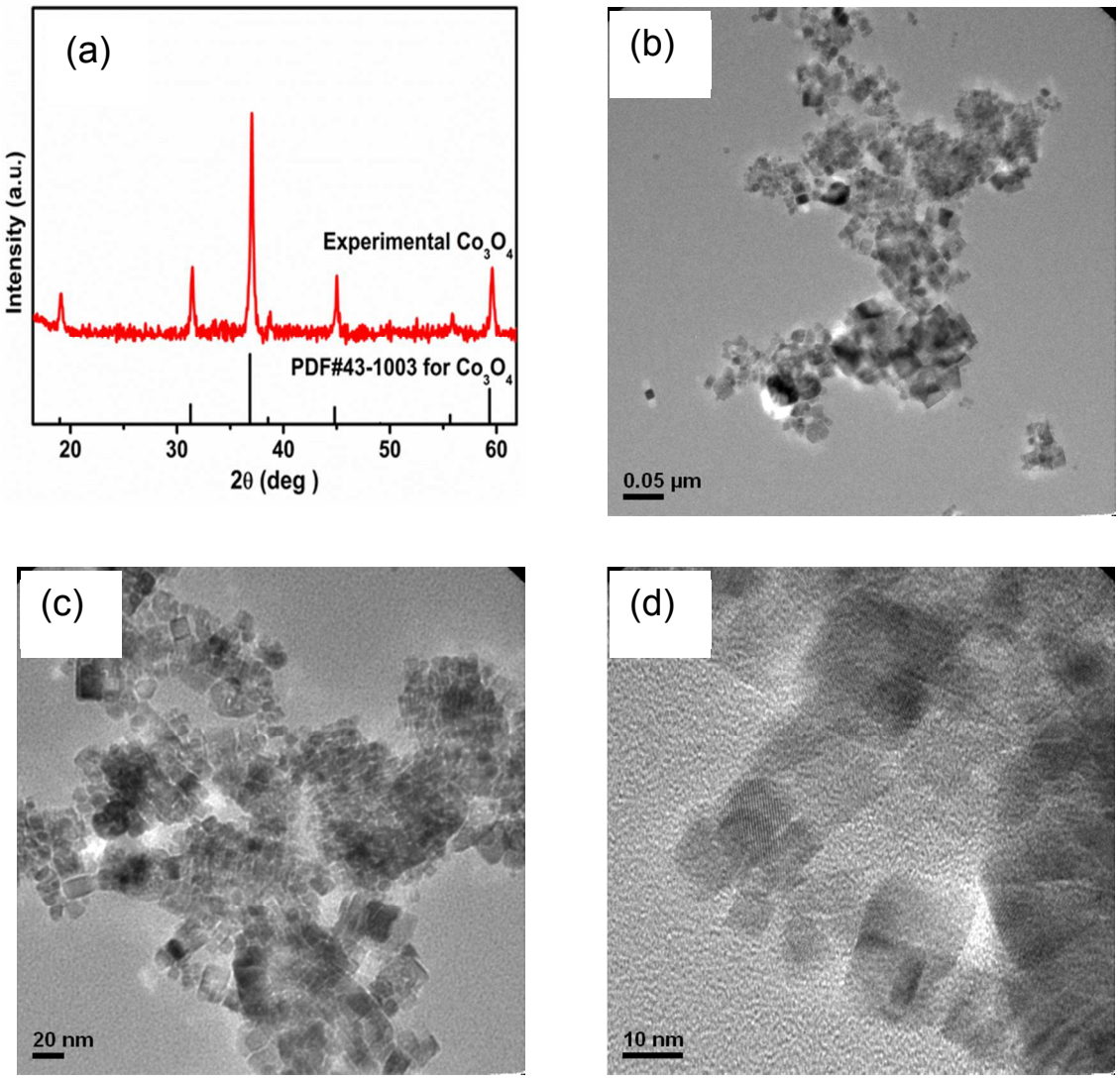

Fig. S9 Standard line pattern (PDF#43-1003) and experimental XRD powder pattern (a), and TEM images (b, c, d) of Co_3O_4.

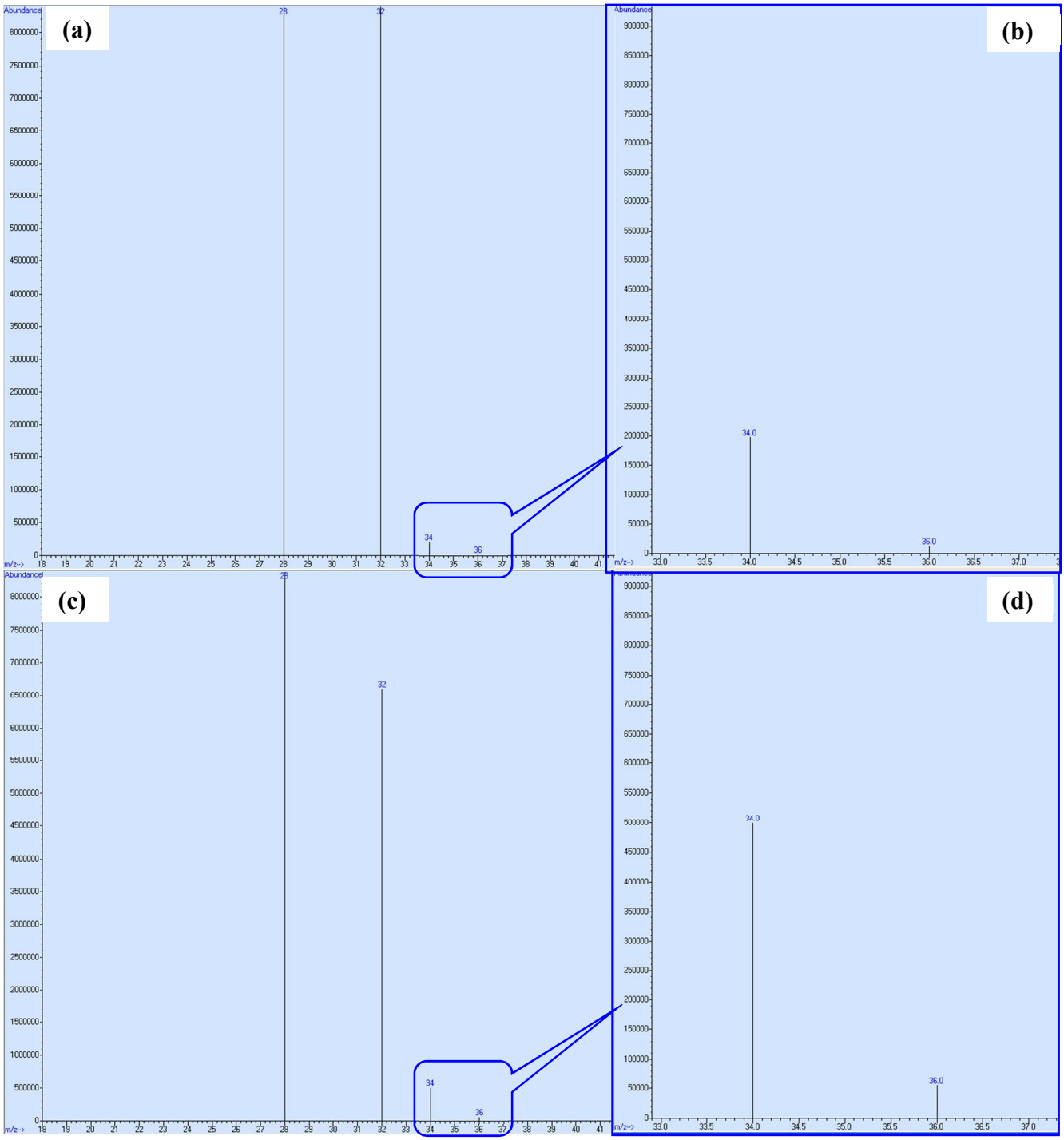

Fig. S10 EI mass spectrum of air (100 μL) (*a*, *b*) and the gas sample evolved (100μL) (*c*, *d*) during photocatalysis using sample **1** in $^{18}OH_2$-enriched borate buffer solution (16.8%, $^{18}OH_2$).

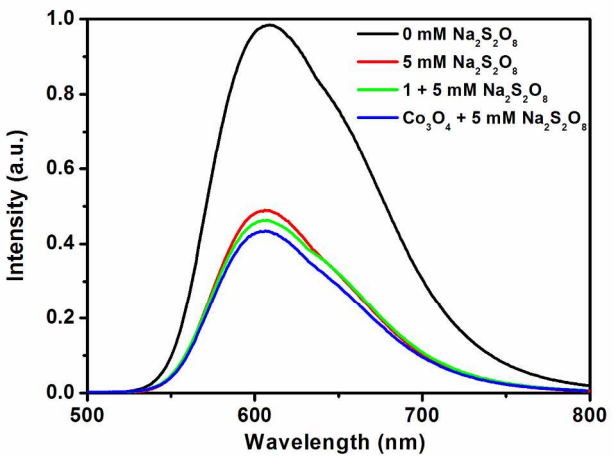

Fig. S11 Steady-state luminescence spectra of $[Ru(bpy)_3]^{2+}$ in the presence and absence of 5.0 mM persulfate; and in the presence of 5.0 mM persulfate and the catalyst (**1** and Co_3O_4) (λ_{ex} = 450 nm). Conditions: 1.0 mM $[Ru(bpy)_3]^{2+}$, 40 mM borate buffer (initial pH 9.0), 0.14 g L^{-1} catalyst.

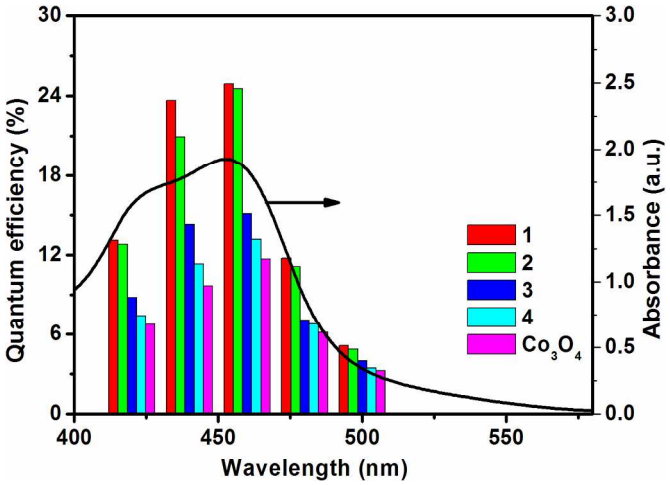

Fig. S12 The quantum efficiencies of O_2 evolved under light-irradiation at different wavelength of 420, 440, 460, 480, and 500 nm over different cobalt phosphonates (**1-4**) and Co_3O_4 control (0.14 g L^{-1}) and UV-vis absorption spectrum of $Ru(bpy)_3Cl_2$. Conditions: 1.0 mM $[Ru(bpy)_3]^{2+}$, 5.0 mM $Na_2S_2O_8$, 40 mM borate buffer (initial pH 9.0), total volume of the reaction solution 100 mL, light source: 300 W Xe lamp with different wavelength cut-off filter. It is to note that only a small amount of oxygen was generated with the band-pass filter. To obtain more accurately data, the total reaction solution volume was increase to 100 mL with other conditions kept the same.

Comments:

In the water oxidation system using $[Ru(bpy)_3]^{2+}$ as a photosensitizer and $Na_2S_2O_8$ as a two-electron acceptor, the overall reaction can be expressed as:

$$2H_2O + 2Na_2S_2O_8 \rightarrow O_2 + 4H^+ + 4Na^+ + 4SO_4^{2-} \quad (1)$$

This suggests that in any condition, the theoretical maximum amount of O_2 produced should correspond to half of the amount of persulfate added.

During photocatalytic water oxidation, the photoexcitation of $[Ru(bpy)_3]^{2+}$ generates $[Ru(bpy)_3]^{3+}$ by the oxidative quenching of the metal-ligand charge-transfer (MLCT) excited state $[Ru(bpy)_3]^{2+*}$ with $Na_2S_2O_8$. The absorption of two photons and the consumption of 2 equiv. of $Na_2S_2O_8$ results in the formation of 4 equiv. of $Ru(bpy)_3]^{3+}$ as shown in equation (2). Hence, the quantum efficiency of O_2 formation is defined as the number of O_2 molecules formed per two absorbed photons.

$$4[Ru(bpy)_3]^{2+} + 2Na_2S_2O_8 + 2h\nu \rightarrow 4Ru(bpy)_3]^{3+} + 4Na^+ + 4SO_4^{2-} \quad (2)$$

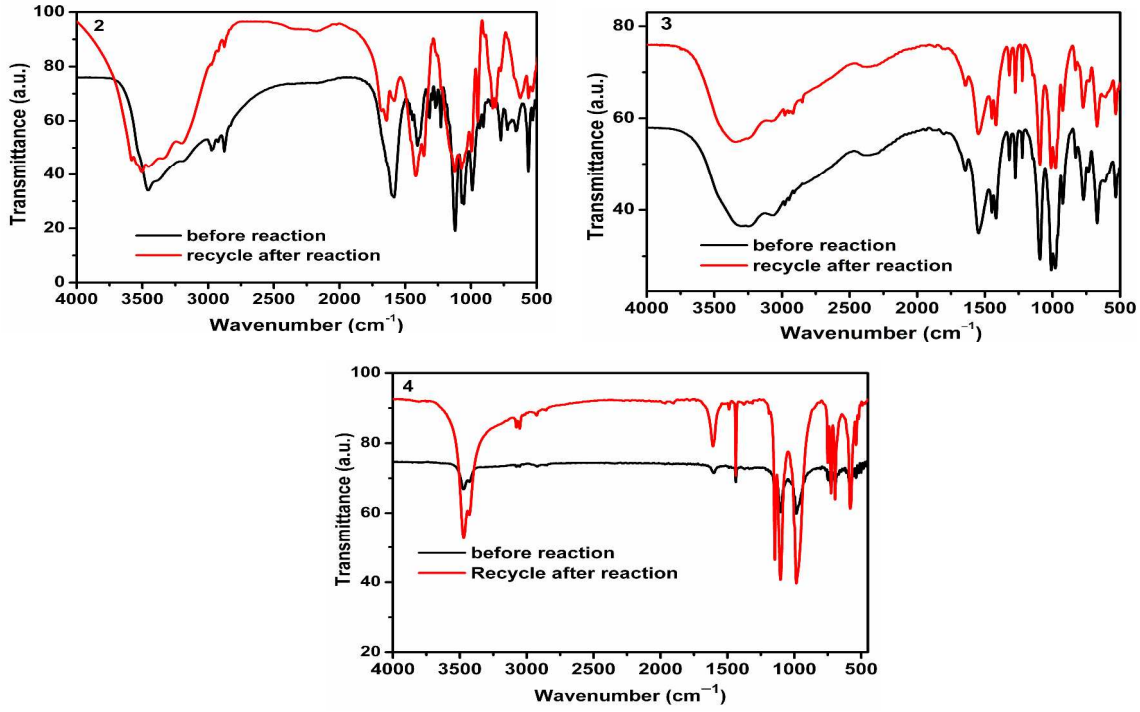

Fig. S13 FTIR spectra of cobalt phosphonates before and after photoreaction.

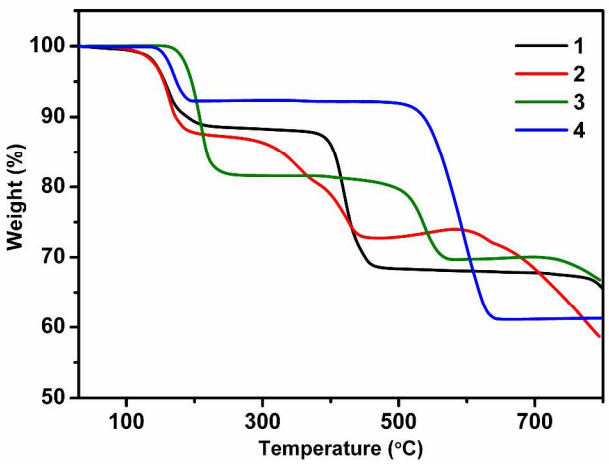

Fig. S14 TGA results of cobalt phosphonates.

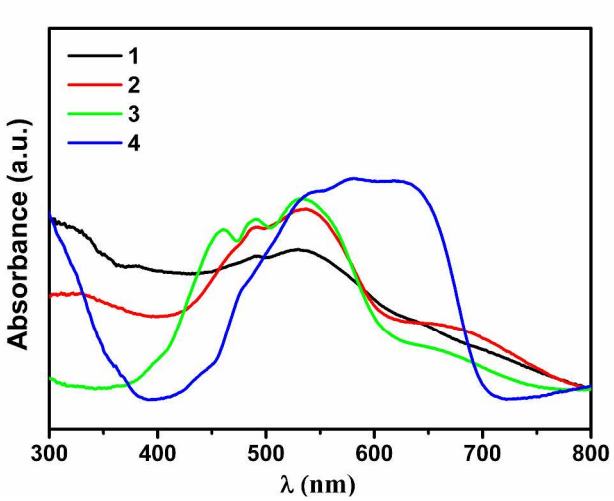

Fig. S15 UV-Vis diffuse reflectance spectra (DRS).

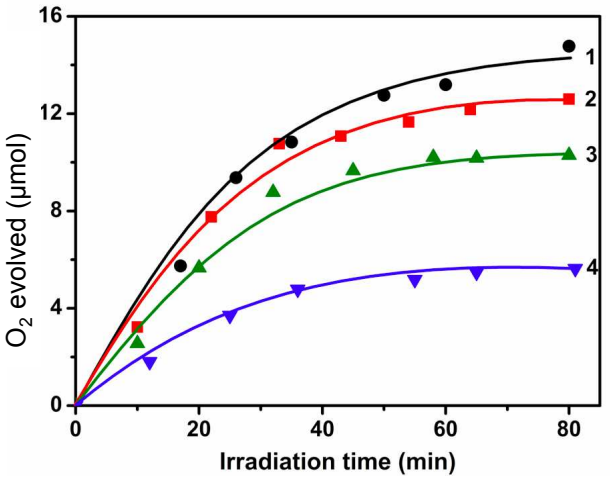

Fig. S16 O_2 production over the as-synthesized crystal samples **1-4** without grinding (0.14 g L^{-1}). Conditions: 1.0 mM $[Ru(bpy)_3]^{2+}$, 5.0 mM $Na_2S_2O_8$, 40 mM borate buffer (initial pH 9.0), total volume of the reaction solution 10 mL, light source: 300 W Xe lamp with 420 nm cut-off filter.

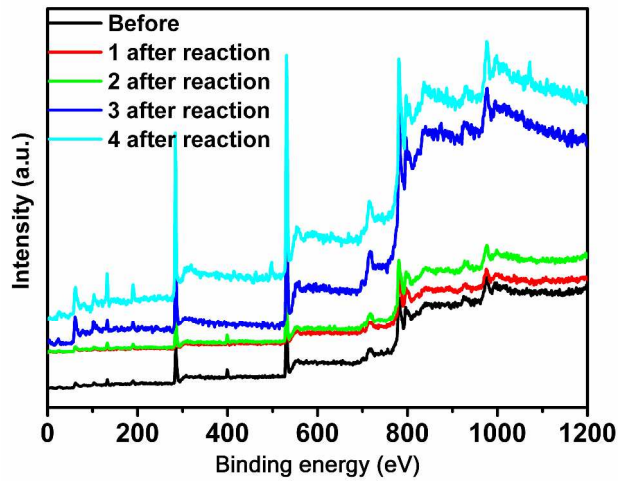

Fig. S17 XPS survey scans of **1-4** after photocatalytic reaction and **1** before reaction.

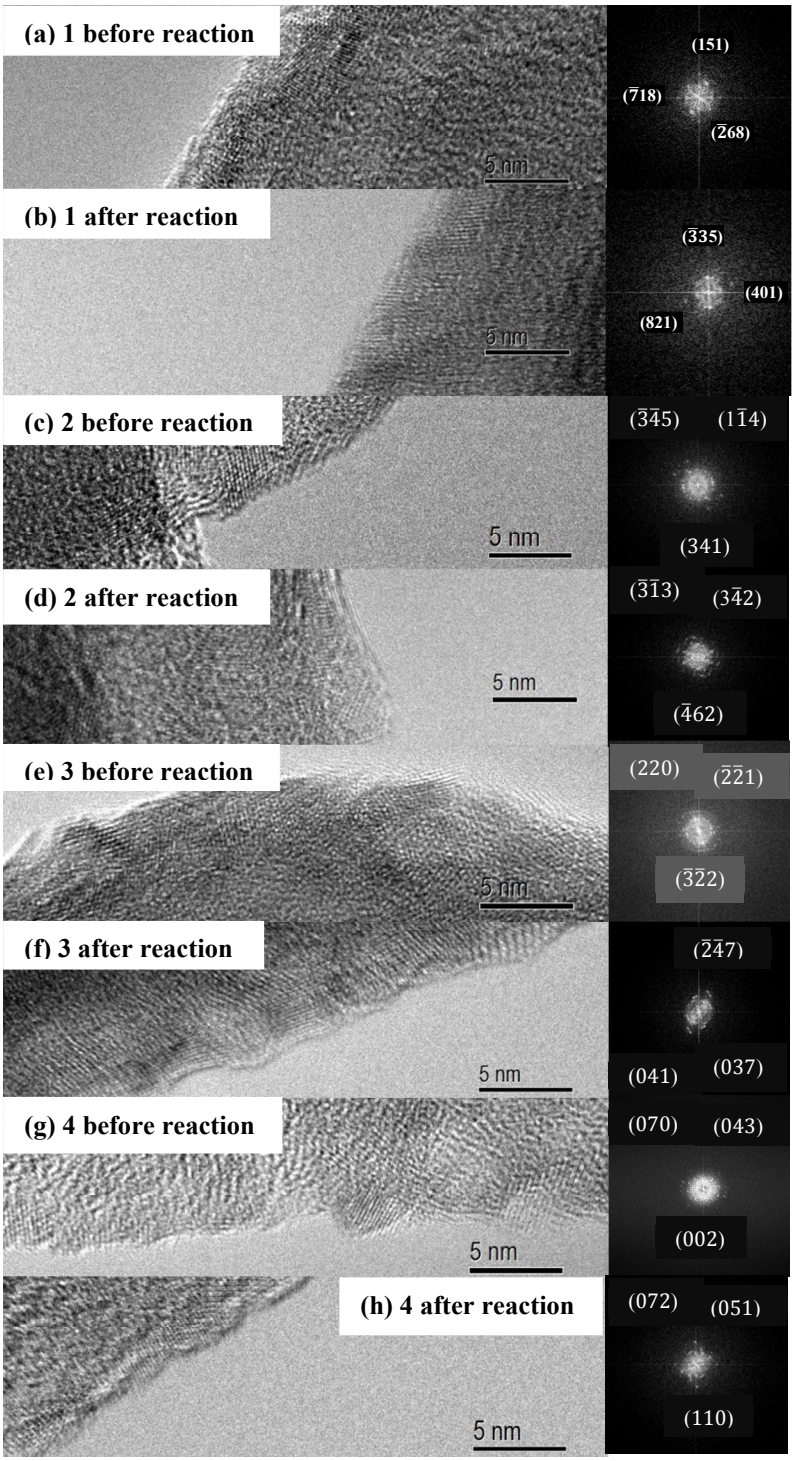

Fig. S18 HRTEM images (left) and FFTs (right) of surface regions of **1**-**4** before and after photocatalysis. Photocatalytic reaction conditions: cobalt phosphonates **1-4** (0.14 g L^{-1}), 1.0 mM $[Ru(bpy)_3]^{2+}$, 5.0 mM $Na_2S_2O_8$, 40 mM borate buffer (initial pH 9.0), total volume of the reaction solution 10 mL, light source: 300 W Xe lamp with 420 nm cut-off filter.

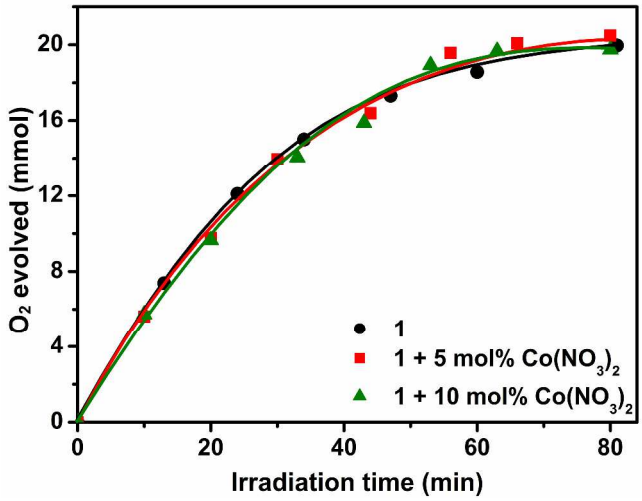

Fig. S19 O_2 evolution over **1** (0.14 g L^{-1}), and the mixture of **1** and $Co(NO_3)_2$. Conditions: 1.0 mM $[Ru(bpy)_3]^{2+}$, 5.0 mM $Na_2S_2O_8$, 40 m Mborate buffer (initial pH 9.0), total volume of the reaction solution 10 mL, light source: 300 W Xe lamp with 420 nm cut-off filter.

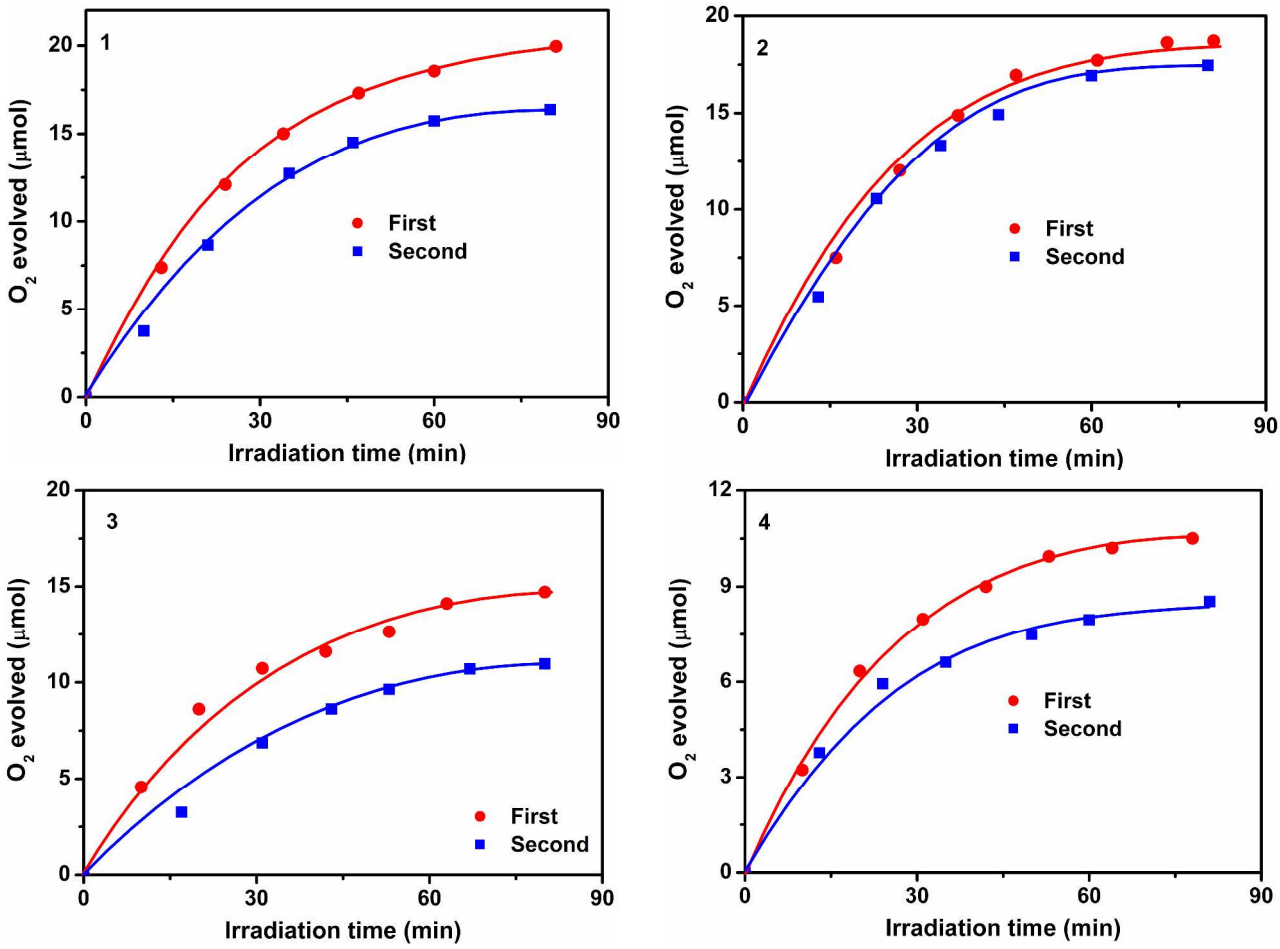

Fig. S20 O_2 production over the fresh sample and recycled sample of **1**-**4** (0.14 g L^{-1}). Conditions: 1.0 mM $[Ru(bpy)_3]^{2+}$, 5.0 mM $Na_2S_2O_8$, 40 mM borate buffer (initial pH 9.0), total volume of the reaction solution 10 mL, light source: 300 W Xe lamp with 420 nm cut-off filter.

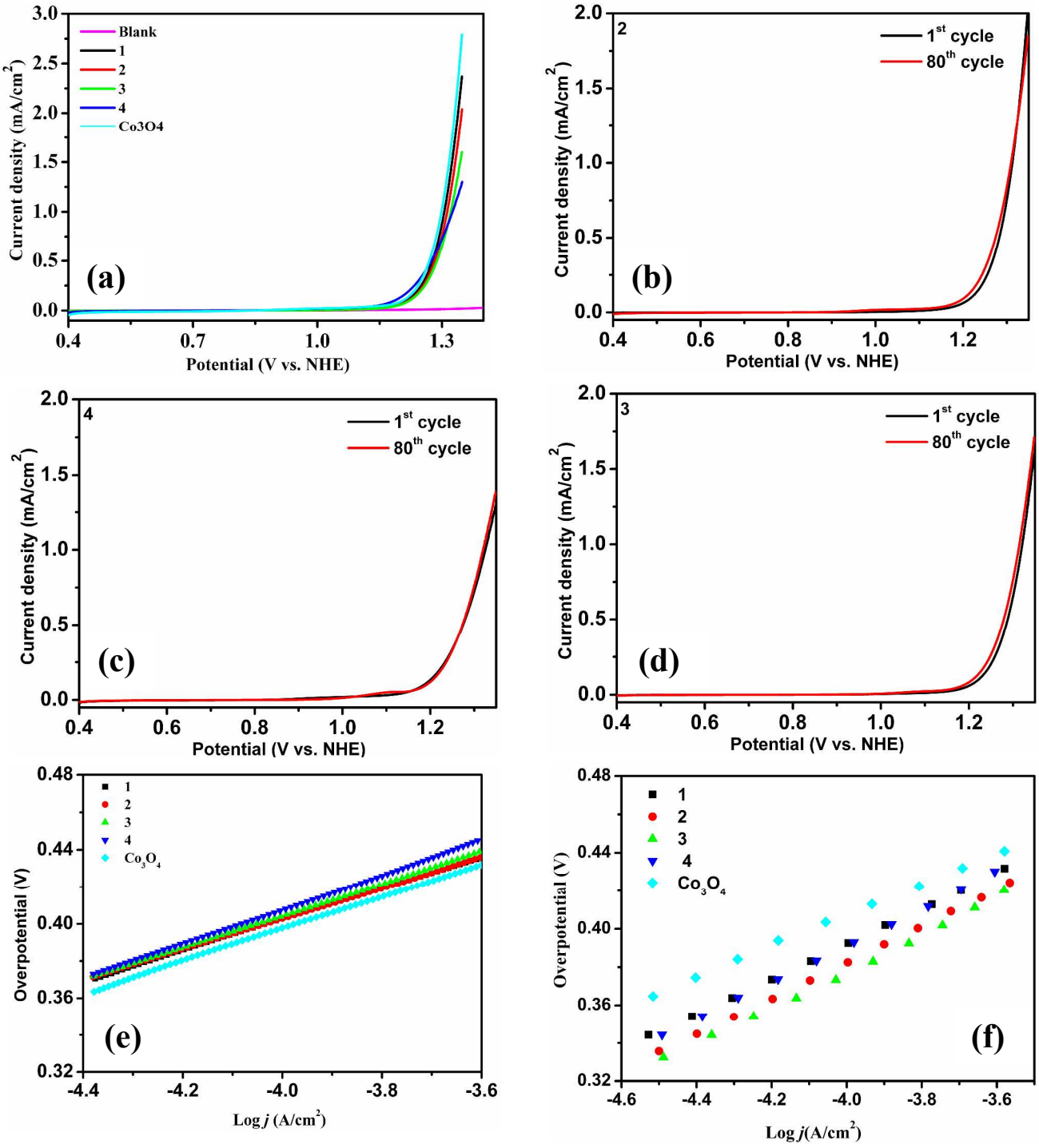

Fig. S21 (a) LSV curves of layered cobalt phosphonates and control Co_3O_4, LSV curves of 2 (b), 3 (c), and 4 (d) showing the first and 80th cycles, and Tafel plots obtained by LSV (e) and steady state data (f). All results were obtained in 0.1 M phosphate buffer solution (pH 7.0).

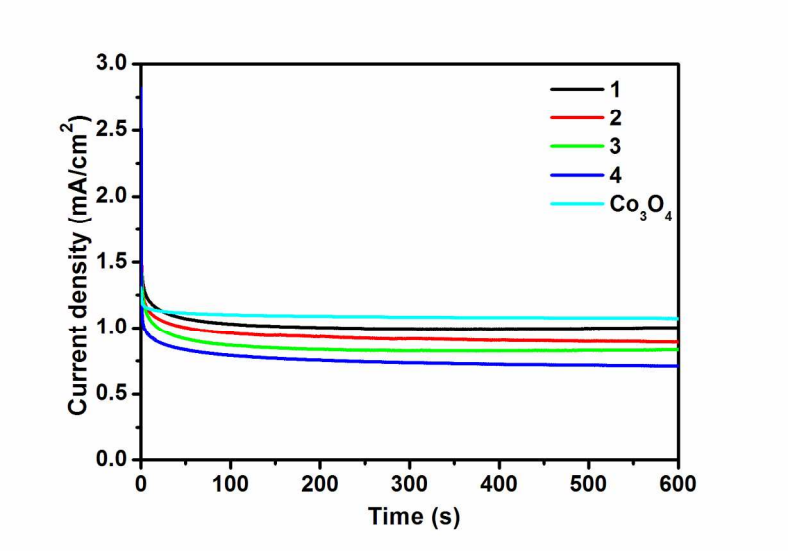

Fig. S22 Chronoamperometric *i*-t curves obtained with cobalt phosphonates modified glass carbon electrodes. Electrolysis experiments were carried out in 0.1 M phosphate buffer solution (pH 7.0) at a constant applied potential of +1.3 V versus NHE. During the measurement, the electrode was rotated at a rate of 1600 rpm to remove O_2 bubbles formed from the electrode surface and the pH was remained unchanged in the longer timescale experiments.

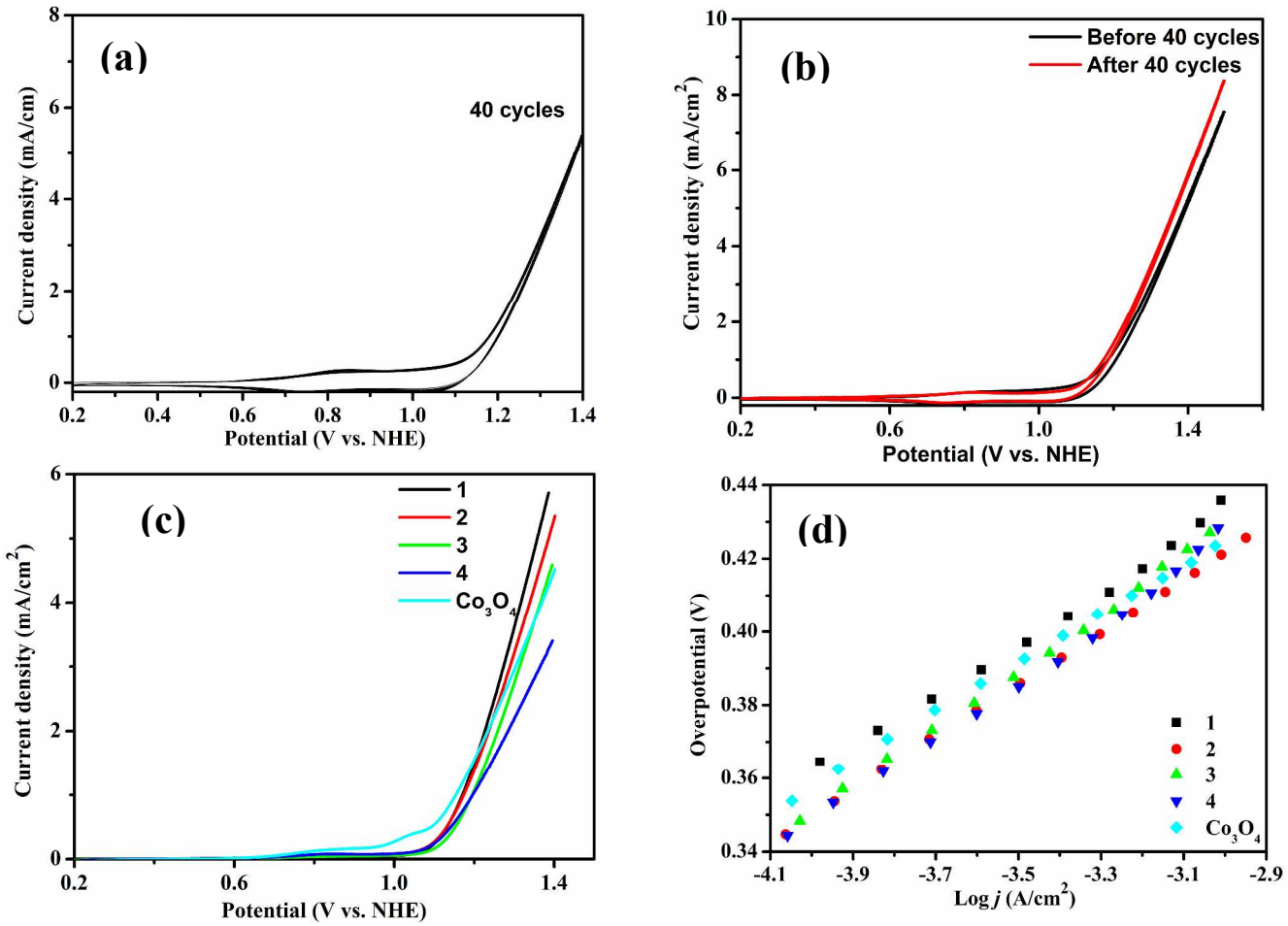

Fig. S23 (a) CV scans of **1** from 0.2 to 1.4 V at a scan rate of 100 mV/s for continuous cycles, (b) CVs of **1** at a scan rate of 20 mV/s from 0.2 to 1.5 V before and after 40 continuous cycles, (c) LSV curves of **1-4** and Co_3O_4, and (d) Tafel plots obtained from steady state data. All results were obtained at 1600 rpm in 40m Mborate (pH 9.0).

References

S1. B. P. Yang, J. G.Mao, Y. Q. Sun, H. H. Zhao, Clearfield, A. *Eur. J. Inorg. Chem.*2003, 4211-4217.

S2. Y. Liang, Y. Li, H. Wang, J. Zhou, J. Wang. T. Regier, H. Dai, *Nat. Mater.*2011,**10**, 780-786.

S3. S. Yusuf, F. Jiao, *ACS Catal.*2012,**2**, 2753-2760.

S4. CrystalClear v. version 1.3.5 (Rigaku Corp, Woodlands, TX, 1999).

S5. SHELXTL, Crystallographic Software Package version 5. 1 (Bruker-AXS, Madison, WI, 1998).

S6. A. Turner, P.-A. Jaffres, E. J. MacLean, D. Villemin, V. McKee, G. B. Hix, *Dalton Trans.* 2003, 1314-1319.

S7. A. Distler, S.C. Sevov,*Chem. Commun.*1998,959-960.

S8. T.Q. Salami, X. Fan, P.Y.Zavalij, S. R. J. Oliver, *Dalton Trans*, 2006,1574-1578.

S9. D. Hong, Y. Yamada, T. Nagatomi, Y.Takai, S.Fukuzumi, *J. Am. Chem. Soc.*2012, **134**, 19572.

S10. T. W. Kim, M. A. Woo, M. Regis and K.-S. Choi, *J. Phys. Chem. Lett.*, 2014, 13, 2370-2374.